MICROCOPY RESOLUTION TEST CHART

NATIONAL BUREAU OF STANDARDS 1963-A

(12)

$A A E$

AERONAUTICAL
AND ASTRONAUTICAL
ENGINEERING DEPARTMENT

DTIC
S ELECTE
OCT 2 2 1986
D
D

ENGINEERING EXPERIMENT STATION, COLLEGE OF ENGINEERING, UNIVERSITY OF ILLINOIS, URBANA

(12)

$\rlap{\diagdown}{\diagup}\mathbb{A}\mathbb{A}\mathbb{E}$
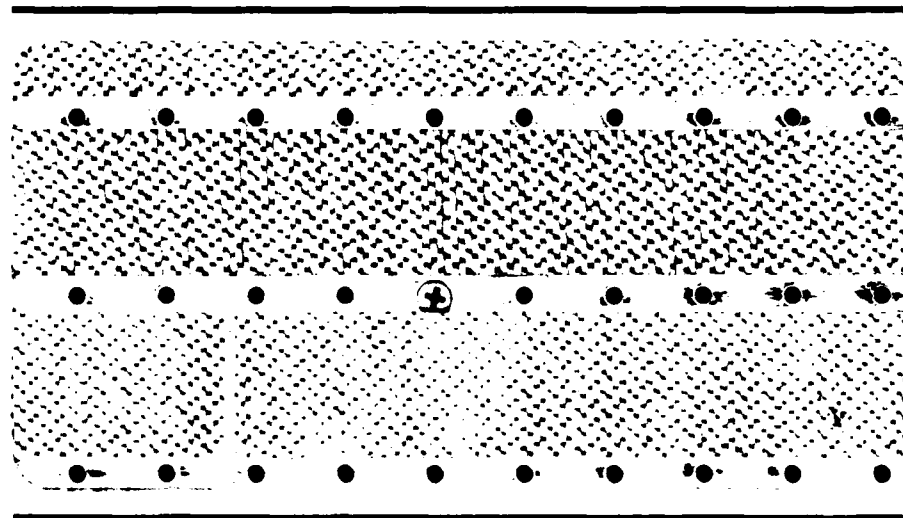
AERONAUTICAL
AND ASTRONAUTICAL
ENGINEERING DEPARTMENT

MASS FLOW CALIBRATION OF THE HELIOS

CLI AND CLII LASER CONTROL CONSOLES

L. H. Sentman, P. Theodoropoulos and A. Gumus

DTIC

S ELECTE

OCT 2 2 1986

D

D

ENGINEERING EXPERIMENT STATION, COLLEGE OF ENGINEERING, UNIVERSITY OF ILLINOIS, URBANA

86 1

Aeronautical and Astronautical Engineering Department

University of Illinois at Urbana-Champaign

Urbana, Illinois

Technical Report AAE TR 86-4

UILU Eng 86-0504

MASS FLOW CALIBRATION OF THE HELIOS

CLI AND CLII LASER CONTROL CONSOLES

L. H. Sentman, P. Theodoropoulos and A. Gumus

Prepared for

Defense Advanced Research Projects Agency

1400 Wilson Blvd.

Arlington, VA 22209

August, 1986

DTIC
ELECTE
OCT 2 2 1986
D

REPORT DOCUMENTATION PAGE

1. REPORT NUMBER	2. GOVT ACCESSION NO.	3. RECIPIENT'S CATALOG NUMBER
AAE 86-4 UILU ENG 86-0504	$AD \cdot A$ /'*) 3 3 $\mathcal{S}$ $\mathcal{f}$	

4. TITLE *(and Subtitle)*	5. TYPE OF REPORT & PERIOD COVERED
Mass Flow Calibration of the Helios CLI and CLII Laser Control Consoles	Technical Report
	6. PERFORMING ORG. REPORT NUMBER

7. AUTHOR(s)	8. CONTRACT OR GRANT NUMBER(s)
L.H. Sentman, P. Theodoropoulos and A. Gumus	N00014-85-K-0326

9. PERFORMING ORGANIZATION NAME AND ADDRESS	10. PROGRAM ELEMENT, PROJECT, TASK AREA & WORK UNIT NUMBERS
Aeronautical and Astronautical Engineering University of Illinois at Urbana-Champaign Urbana, IL 61801	

11. CONTROLLING OFFICE NAME AND ADDRESS	12. REPORT DATE
Defense Advanced Research Projects Agency 1400 Wilson Boulevard Arlington, VA 22209	August 1986
	13. NUMBER OF PAGES

14. MONITORING AGENCY NAME & ADDRESS(*if different from Controlling Office*)	15. SECURITY CLASS. *(of this report)*
Office of Naval Research Resident Representative Room 286, 536 S. Clark Street Chicago, IL 60605	UNCLASSIFIED
	15a. DECLASSIFICATION DOWNGRADING SCHEDULE

16. DISTRIBUTION STATEMENT *(of this Report)*

UNLIMITED

17. DISTRIBUTION STATEMENT *(of the abstract entered in Block 20, if different from Report)*

18. SUPPLEMENTARY NOTES

19. KEY WORDS *(Continue on reverse side if necessary and identify by block number)*

Chemical laser
Mass flow measurement
Mass flow meter choking
Laminar to turbulent transition in an orifice

20. ABSTRACT *(Continue on reverse side if necessary and identify by block number)*

Calibration curves of laser control console pressure versus mass flow rate for the four input species H_2, SF_6, O_2 and He were measured for the single and two channel laser control consoles. Several interesting phenomena were observed. The mass flow meter choked unless placed upstream of the flow control orifice and a laminar to turbulent transition occurred in the flow control orifice.

DD FORM 1 JAN 73 **1473**   EDITION OF 1 NOV 65 IS OBSOLETE

TABLE OF CONTENTS

I.   INTRODUCTION

This research is an integrated experimental and theoretical investigation of the multi-line issues associated with assessing the impact of temporal variations in a CW HF device on the capability of achieving a phased output beam from multiple laser cavities. The objectives of this research are to fully characterize the output of an oscillator-amplifier (MOPA) configuration as a function of the oscillator input beam, time-dependent oscillations, mode beats, and determine if the coupling between the oscillator and amplifier perturbs the oscillator output; these studies are to be carried out for first one and then two amplifiers driven by the same oscillator. To accomplish these objectives, the flow fields in the oscillator and amplifiers must be identical; to ensure that this is so, the devices must first be fully characterized as oscillators (power, power spectral distributions, beam diameters, time-dependent oscillations as a function of cavity losses, pressure and flow rates) including simulation of their performance with computer models. This background information is essential to the interpretation and guidance of the MOPA experiments.

The laser which will be used as the oscillator is a single channel Helios cw HF laser and the lasers which will be used as the amplifiers are two channel Helios cw HF lasers. The flow channels in the two channel laser are identical to each other and to the flow channel in the single channel laser. Thus, the flow fields and hence, the gain distributions in the oscillator and the amplifiers will be identical when the single channel CL I laser is run at one half the flow rates at which the two channel CL II is run. To insure that the flow fields in the single and two channel devices are matched, the mass flow rates of the input species must be known as a function of the console

pressure for each species for both of these lasers. Mass flow calibration curves as a function of control console pressure were measured for each of the input species for each laser. In Section II, the flow system is described, the theory of choked orifice flow control is presented and the principles on which the mass flow meter operates are given. The mass flow calibration experiments and the resulting calibration curves are presented in Section III. Several concluding remarks are given in Section IV.

II. DESCRIPTION OF THE FLOW SYSTEM

To insure that the flow field in the single channel CL I laser duplicates the flow field in the two channel CL II laser, the single channel laser must be operated at one half the mass flow rate of the two channel laser. The ability to do this is essential in order to study the effect of match/mismatch of the oscillator/amplifier flow fields on MOPA performance.

A schematic of the flow system, which is the same for both the CL I and the CL II lasers, is shown in Fig. 1. The mass flow of each species is controlled by an orifice in the flow line which is downstream of a needle valve that is used to set the supply pressure for the orifice. The supply pressure for the orifice is read on a pressure gage on the laser control console. Mass flow rates were measured using a Micro Motion[1] Mass Flow Meter. Initially, the mass flow meter (MFM) was placed at position B (Fig. 1), which was located downstream of the orifice. Position B was chosen simply because it was convenient at the time. However, during the course of the experiments, the data showed that the MFM had to be moved to Position A (Fig. 1), which was located upstream of the orifice. Location B will be referred to as "downstream" and location A as "upstream".

2.1 Choked Orifice Theory

Since the pressure in the laser is always lower than the pressure set on the gas bottle regulator valve, the mass flow rate through the system is determined by the orifice supply pressure which is set by the control console needle valve. Since the orifice is a converging nozzle, the mass flow rate through the orifice is given by[2]

$$\dot{m} = \sqrt{\frac{\gamma}{RT_t}} \quad \frac{M_e \, P_t \, A_e}{\left[1 + \frac{\gamma-1}{2} M_e^2\right]^{\frac{\gamma+1}{2(\gamma-1)}}} \qquad (2.1\text{-}1)$$
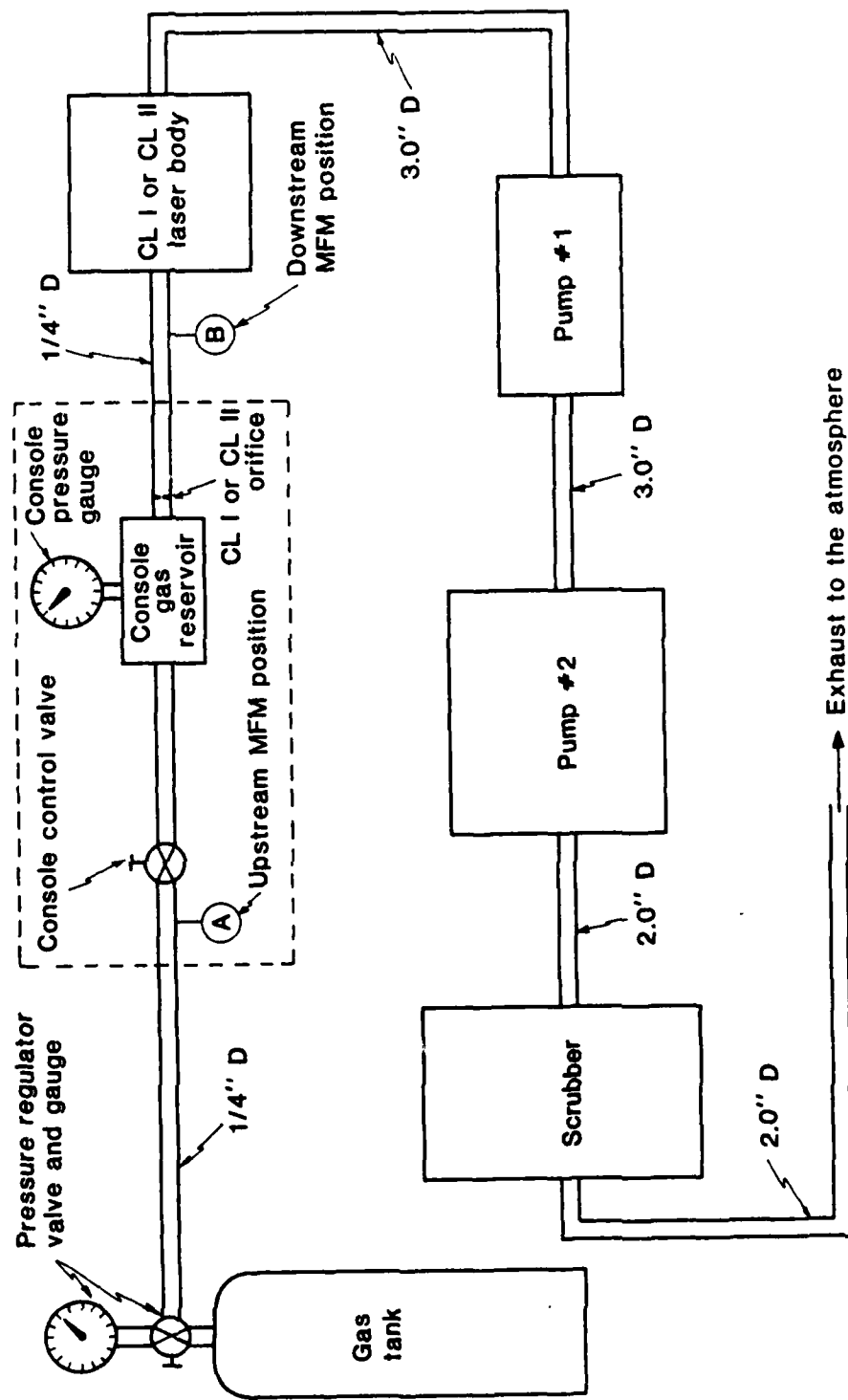
Figure 1. Schematic of the laser mass flow system.

where M_e is the Mach number at the orifice exit plane, A_e is the area of the orifice exit plane, P_t is the resevoir pressure, T_t is the resevoir temperature, γ is the specific heat ratio and R is the gas constant for the particular species. Equation (2.1-1) assumes the flow from the resevoir, where the velocity is approximately zero, to the orifice exit plane is isentropic. Since the flow system is designed so that the cross sectional area of the plenum where the console pressure gage measures the pressure is much larger than the orifice area, the velocity in the plenum will be very small and the console pressure is approximately P_t, the total pressure for the orifice flow. Since the pressure in the orifice plenum starts at zero when the needle valve is closed, as the needle valve is opened, the flow begins with the Mach number everywhere subsonic. The mass flow rate is determined by the boundary condition that the pressure at the orifice exit must equal the back pressure P_b. As the needle valve opens further, the plenum pressure rises and the Mach number at the orifice exit increases until it eventually reaches 1; at this point the orifice is choked. Further increases in P_t do not change M_e. When this occurs, Eq. (2.1-1) becomes

$$\dot{m} = \sqrt{\frac{\gamma}{RT_t}} \; P_t \; A_e \; \left(\frac{2}{\gamma+1}\right)^{\frac{\gamma+1}{2(\gamma-1)}} \qquad (2.1-2)$$

Thus, once the orifice is choked, $\dot{m}$ is a linear function of P_t. The value of the pressure at the orifice exit when the orifice is choked is called the critical pressure, P_*, and since

$$\frac{P_e}{P_t} = \left[1 + \frac{\gamma-1}{2} M_e^2\right]^{-\frac{\gamma}{\gamma-1}} \qquad (2.1-3)$$

the critical pressure ratio at which the orifice chokes is given by

$$\frac{P_*}{P_t} = \left(\frac{\gamma+1}{2}\right)^{-\frac{\gamma}{\gamma-1}}$$
(2.1-4)

When $\frac{P_b}{P_t} > \frac{P_*}{P_t}$, the orifice is not choked and when $\frac{P_b}{P_t} < \frac{P_*}{P_t}$, the orifice is choked and $P_e = P_* > P_b$. There will be no flow until $P_t > P_b$. Then as P_t increases, $\dot{m}$ increases until $P_b/P_t = P_*/P_t$, at which point the orifice chokes and $\dot{m}$ is then a linear function of P_t. This behavior is illustrated in Fig. 2. If the back pressure were zero, then the orifice would choke for arbitrarily small values of P_t and the plot of P_t versus $\dot{m}$ would extrapolate back to the origin as shown by the dotted line in Fig. 2. This fact will be useful later in correcting the zero point of the mass flow meter.

From the preceding discussion, a plot of console pressure versus $\dot{m}$ should be a straight line once the orifice is choked.

Before proceeding to the mass flow data, a description of the mass flow meter and its principle of operation will be given.

2.2 Operation of the Mass Flow Meter

Operation of the Micro Motion MFM is most easily explained by referring to Fig. 3. As _mass travels longitudinally through the pipe with a velocity $\vec{V}$, a Coriolis force $\vec{F}_c$ is present that tends to rotate the pipe about an axis that is parallel to the axis of the earth's rotation. The magnitude of this force $\vec{F}_c$, which is extremely small, is given by the relation[3]

$$\vec{F}_c = 2 M \vec{\omega} \times \vec{V}$$
(2.2-1)

where M is the mass of the fluid in the pipe, $\vec{\omega}$ is the angular velocity of the earth, $\vec{V}$ is the velocity of the fluid in the pipe, and X denotes the vector cross product. The Coriolis force is also present in the case of an
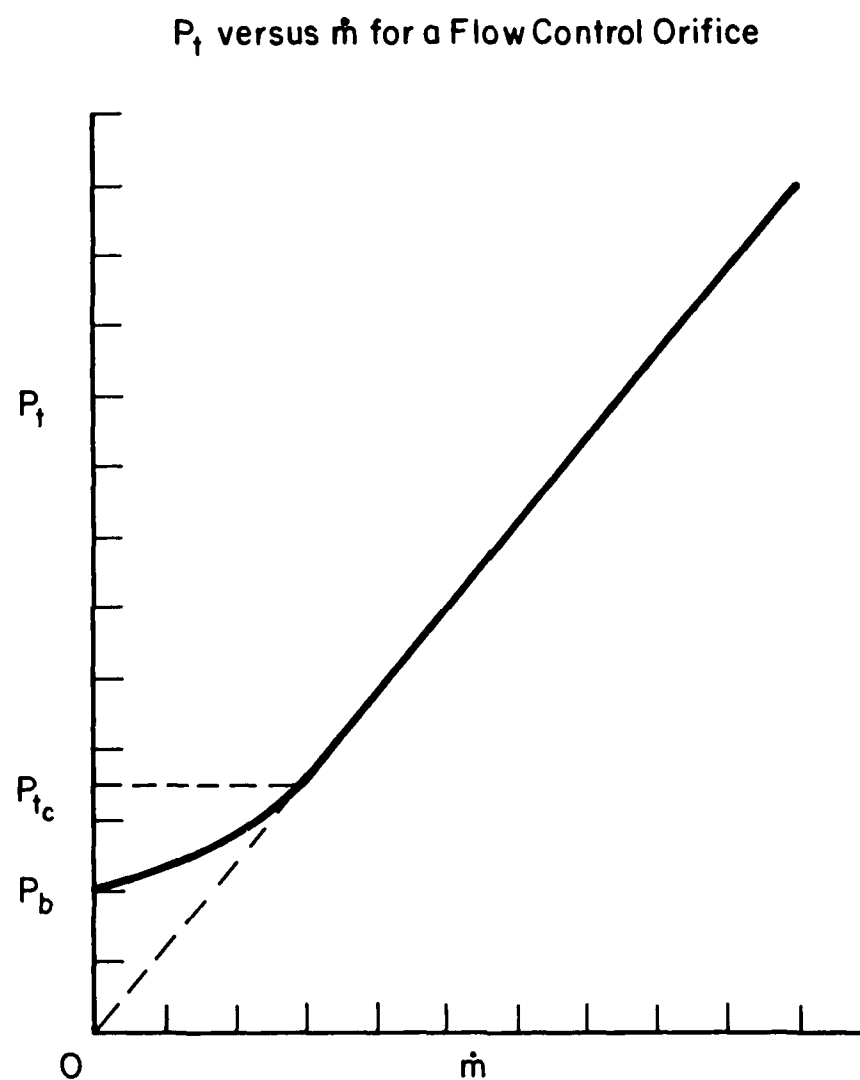
P_t versus $\dot{m}$ for a Flow Control Orifice

Figure 2. Sketch of P_t versus $\dot{m}$ for an orifice controlled flow system. The value of P_t at which the orifice first chokes is denoted by P_{t_c}; P_{t_c} is equal to $P_b/(P_*/P_t)$ where P_b is the pressure in the region immediately downstream of the orifice exit.
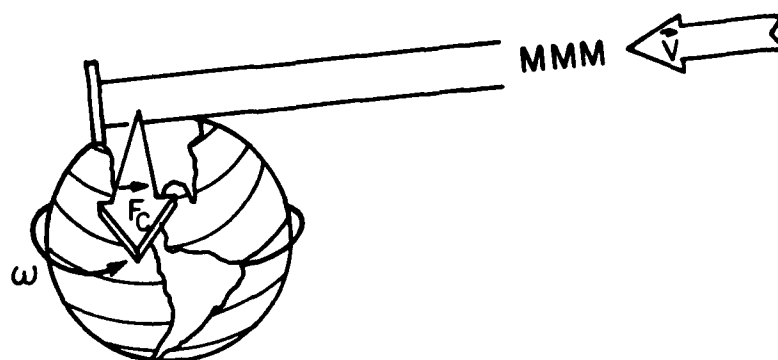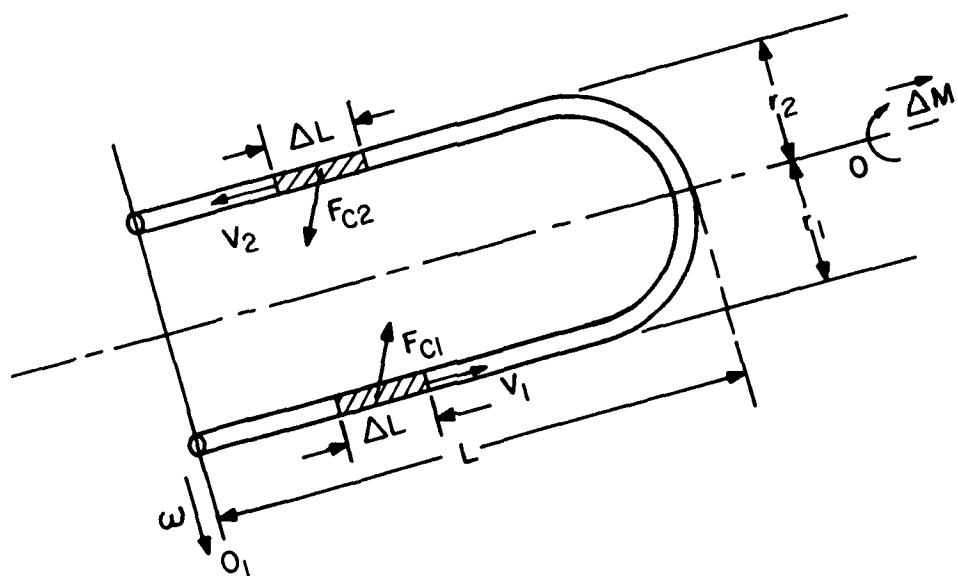
Figure 3. Illustration of Coriolis force.

Figure 4. In operation, the mass flow meter forces F_{c1} and F_{c2} create an oscillating movement, ΔM, about axis 0.

oscillatory motion instead of a rotational motion. The associated Coriolis force $\vec{F}_c$ is now an oscillatory force.

Figure 4 shows the U-shaped pipe which acts as the sensor of the MFM, the axis of oscillation O_1 and a unit length of fluid within each leg of the pipe It can be seen that the velocity vectors $\vec{V}_1$ and $\vec{V}_2$ are perpendicular to the angular rotation vector $\vec{\omega}$, and that the Coriolis force vectors $\vec{F}_{c1}$ and $\vec{F}_{c2}$ are in opposite directions since the velocity vectors, $\vec{V}_1$ and $\vec{V}_2$, are in opposite directions. When the flow meter is in operation, the U shaped tube vibrates about the axis O_1. Thus, the angular velocity $\vec{\omega}$ is a sinusoidal function, and the forces $\vec{F}_{c1}$ and $\vec{F}_{c2}$ are sinusoidal and 180 deg. out of phase with each other. Forces $\vec{F}_{c1}$ and $\vec{F}_{c2}$ create an oscillating moment $\Delta\vec{M}_1$ about axis 0, as illustrated in Fig. 4. The moment can be expressed as a force times a distance,

$$\Delta M_1 = F_{c1}r_1 + F_{c2}r_2 \tag{2.2-2}$$

If the U shaped tube is symmetrical about the axis 0, the two terms are equal and

$$\Delta M_1 = 2 F_{c1}r_1 = 4 MV_1\omega r_1 \tag{2.2-3}$$

when Eq. (2.2-1) is used for F_{c1}. Since $M = \rho A \Delta L$ and the mass flow rate through the pipe is given by $\dot{m} = \rho A V_1$, Eq. (2.2-3) can be written as

$$\Delta M_1 = 4 \rho A \Delta L V_1 \omega r_1 = 4 \dot{m} \omega r_1 \Delta L \tag{2.2-4}$$

The total moment, M_1, about axis 0 due to the Coriolis force on all the moving fluid in the pipe is

$$M_1 = \int \Delta M_1 = \int_0^L 4\dot{m}\omega r_1 dL = 4\dot{m}\omega r_1 L \tag{2.2-5}$$

where L is the length of the U shaped pipe.

The moment M_1 due to the Coriolis force causes an angular deflection of the U-shaped pipe about the axis 0, Fig. 5. The deflection angle θ due to the moment M_1 is determined by the spring constant of the U-shaped pipe system. This spring constant is a function of the cantilever stiffness of the longitudinal pipe. For any given pipe system,

$$\text{Torque} = K_s \theta \qquad (2.2\text{-}6)$$

where θ is the pipe-system deflection angle and K_s is the pipe system angular spring constant.

When Eq. (2.2-5) is set equal to (2.2-6), the mass flow rate can be expressed in terms of the deflection angle as

$$\dot{m} = \frac{K_s \theta}{4\omega r_1 L} \qquad (2.2\text{-}7)$$

Thus, the mass flow rate, $\dot{m}$, is directly proportional to the deflection angle, θ, and inversely proportional to the angular velocity, ω, of the U-shaped pipe system. The deflection of the U-shaped pipe is sensed by an optical system which measures the time interval Δt between optical pulses, Fig. 6. Because of the relative positions of the optical sensors and the pipe[1], the deflection of the U-pipe is related to its velocity times the time interval, Δt, between photo-pulses p_1 and p_2 by

$$V_p \Delta t = 2r_1 \theta \qquad \text{or} \qquad \Delta t = \frac{2r_1 \theta}{V_p} \qquad (2.2\text{-}8)$$

where V_p is the velocity of the pipe at the position of the optical pickoffs and Δt is the time interval that photo pickoff p_1 leads or lags p_2. The vertical velocity of the end of the U-pipe is given by

$$V_p = L\omega \qquad (2.2\text{-}9)$$

where L is the length of the U-shaped pipe. Substitution of Eq. (2.2-9) into Eq. (2.2-8) gives
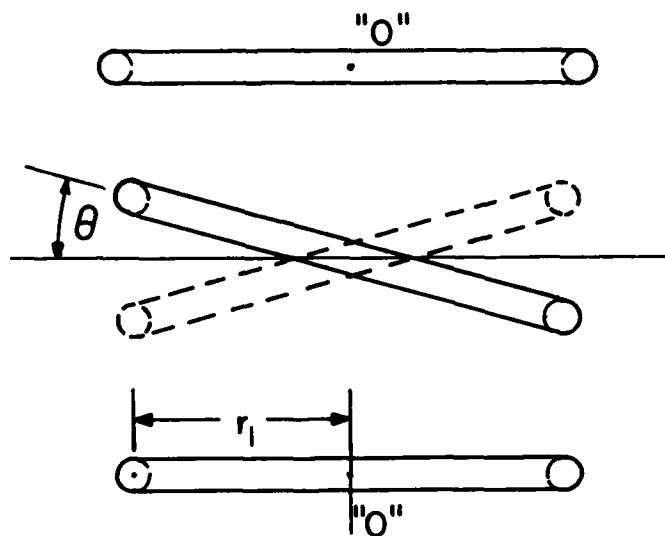
Figure 5.   End view of the U-shaped tube.

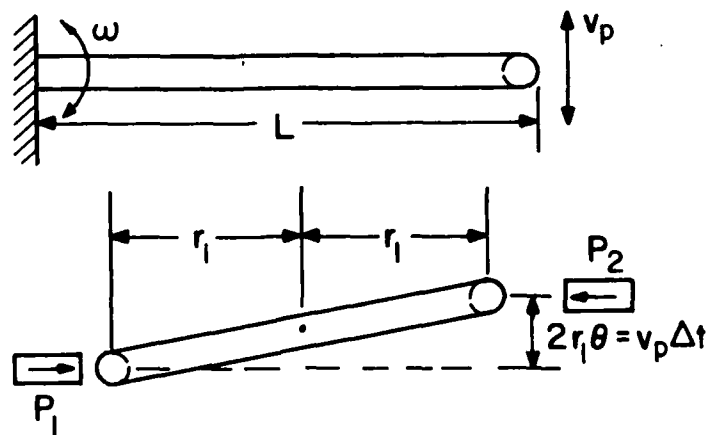Figure 6.   The excursion of the U-pipe can be expressed as
its velocity times the time interval Δt between
photo-pulses P_1 and P_2.

$$\theta = \frac{L\omega\Delta t}{2r_1} \qquad (2.2\text{-}10)$$

Substitution of Eq. (2.2-10) into Eq. (2.2-7) gives

$$\dot{m} = \frac{K_s \; L\omega\Delta t}{8\omega r_1^2 L} = \frac{K_s \Delta t}{8 r_1^2} \qquad (2.2\text{-}11)$$

The mass flow rate is, therefore, a function of pipe geometry, angular spring constant and Δt, the time interval between photo-pulses. This analysis shows that the meter measures mass flow directly independent of the type of fluid. For more information on the operation of the MFM, Ref. 1 should be consulted.

The output signal produced by the MFM is linear from zero up to flow rates which are limited only by the amount of fluid which can pass through a particular size tube. Over nearly all of the range, the signal is accurate to within ± 0.4 percent of the indicated flow rate[1].

III. MASS FLOW DATA

The purpose of the mass flow measurements was to generate a set of curves of console pressure versus mass flow rate for each of the laser gases H_2, He, O_2 and SF_6 for both the CL I and CL II laser control consoles. With these curves, it is possible to select a given flow rate by adjusting the flow control needle valve until the pressure gage reads the pressure corresponding to the desired flow rate. First, the results for the calibration of the CL I hydrogen flow rate will be given. Then the results for the other gases for both the CL I and the CL II will be presented.

3.1 CL I Hydrogen Calibration

The MFM was inserted into the H_2 line at the downstream position B in Fig. 1. The resulting console pressure versus mass flow rate is shown in Fig. 7. Since the flow is controlled by a choked orifice, the break in the slope of console pressure versus mass flow rate was unexpected. The fact that both segments of the curve are straight lines suggests that a change in the controlling area occurred between console pressure, P_c, of 20 to 25 psig at a mass flow rate of about 0.025 gm/sec. The geometry of the flow control orifice #1 is shown in Fig. 8. To determine the role of orifice geometry on the break in the slope of the mass flow curve, the experiments were repeated with orifice #2, Fig. 8, which has the same cross sectional area as orifice #1, but a different shape. The resulting data are shown in Fig. 9. Comparison of Figs. 7 and 9 shows that the lower slopes ($\dot{m} < 0.025$ gm/sec) are identical and the upper slopes are nearly the same with the slope for orifice #2 slightly greater than the slope for orifice #1. Since the slope of P_c vs $\dot{m}$ is inversely proportional to the orifice area (see Eq. 2.1-2), this suggests that the controlling area for the upper orifice #2 curve is slightly less than for
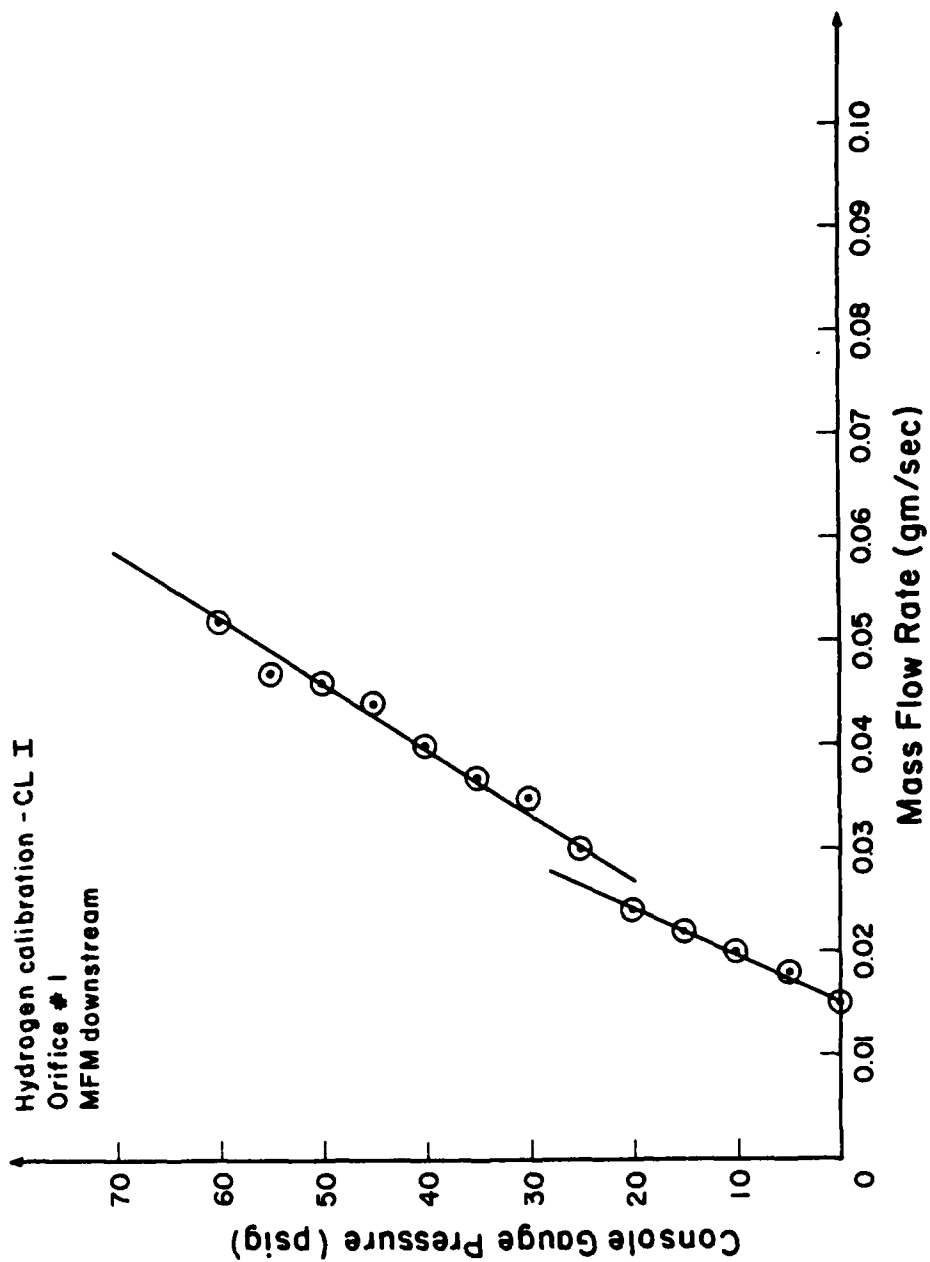
Figure 7. Console pressure versus H_2 mass flow rate for the CL I for orifice #1, with the mass flow meter (MFM) downstream of the flow control orifice.
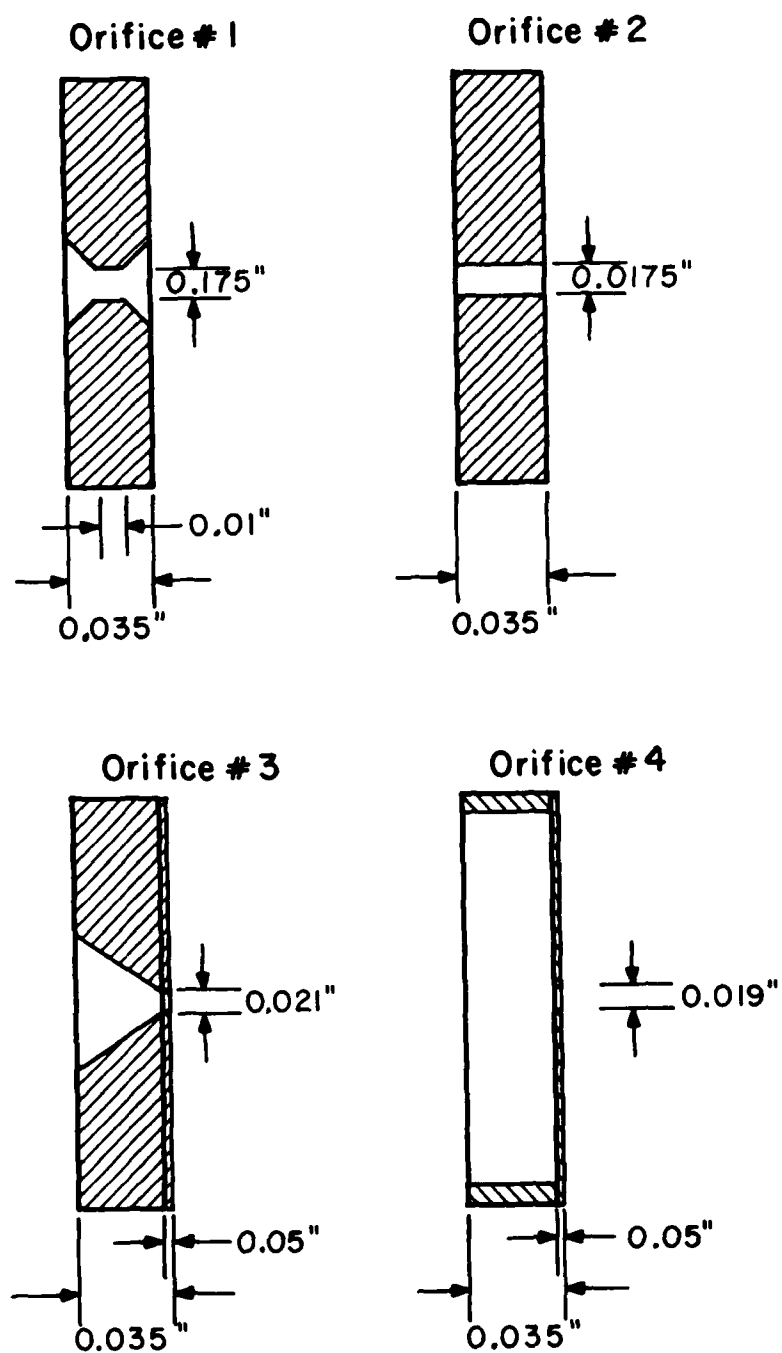
Hydrogen calibration - CL I
Orifice # I
MFM downstream

Console Gauge Pressure (psig)

Mass Flow Rate (gm/sec)

Orifice #1   Orifice #2

0.175"   0.0175"

0.01"

0.035"   0.035"

Orifice #3   Orifice #4

0.021"   0.019"

0.05"   0.05"

0.035"   0.035"

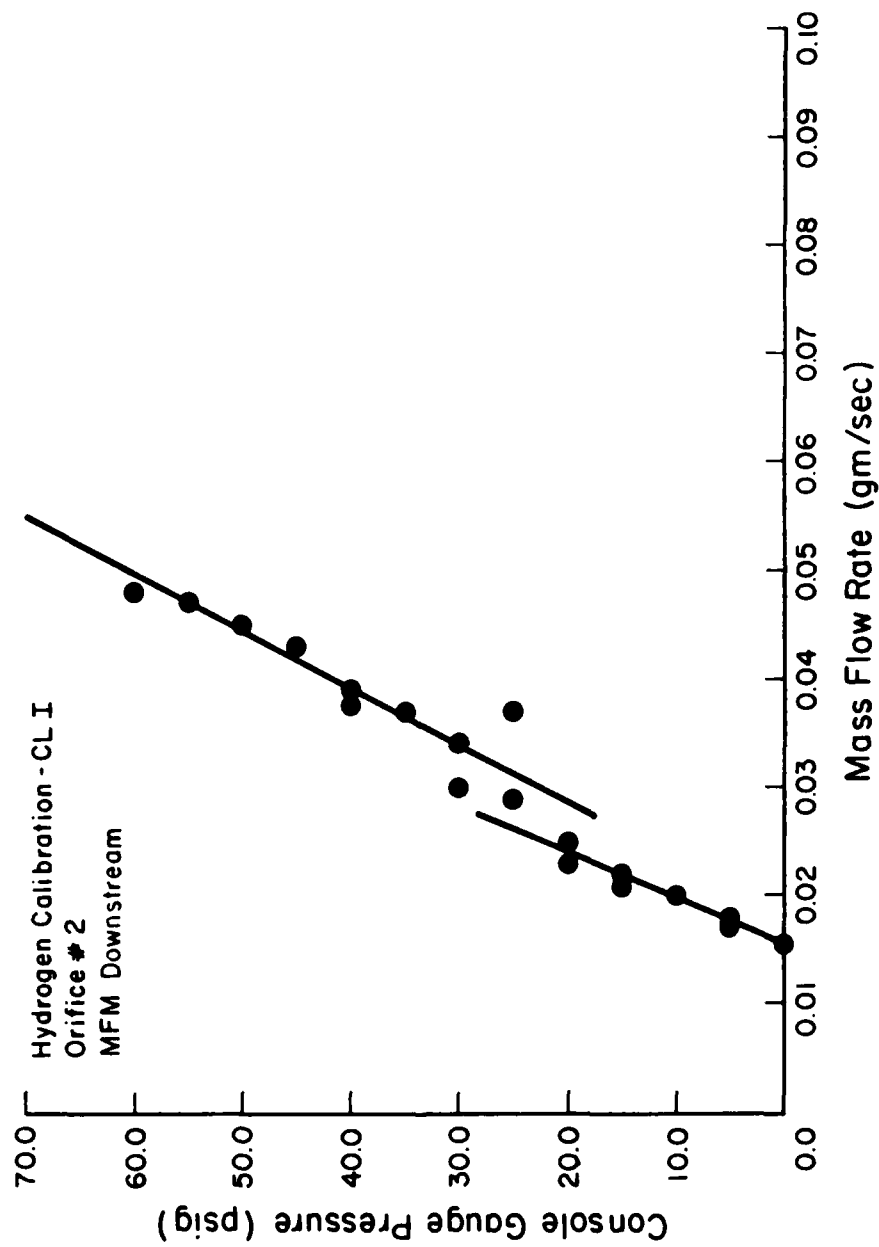Figure 8. Cross-sections of the various CL I H_2 orifices.

Figure 9. Console pressure versus H_2 mass flow rate for the CL I for orifice #2 with the MFM downstream of the flow control orifice.

orifice #1. This is consistent with the fact that the boundary layer in an orifice shaped like #2 would be thicker than in an orifice shaped like #1.

To determine the effect of orifice area, the experiments were repeated with three other orifices: the orifice from the CL I oxygen line whose area is 1.65 times larger than the area of orifice #1; the orifice from the CL I SF_6 line whose area is 2.56 times larger than the area of orifice #1; and an orifice whose area is 0.735 times the area of orifice #1. The results are shown in Figs. 10-12. There are several points to be noted from Figs. 7, 9, 10, 11 and 12. First, the break always occurred at the same mass flow rate, ~ 0.025 gm/sec. Second, the lower slopes ($\dot{m}$ < 0.025 gm/sec) are the same for all orifices. Third, as the orifice area increases, the upper slopes decrease which indicates that the orifice is the controlling area for the upper curves ($\dot{m}$ > 0.025 gm/sec). Thus, some other area, which is independent of the orifice, is controlling the flow when $\dot{m}$ < 0.025 gm/sec.

To determine when the orifice choked, the pressure drop across the orifice was measured, Table 1. Before the orifice chokes, the pressure at the orifice exit must equal the back pressure (pressure downstream of the orifice); once the orifice chokes, the orifice exit pressure will be greater than or equal to the downstream pressure. Since the velocity upstream of the orifice is very small, the console pressure is approximately the total pressure upstream of the orifice. Then the orifice is choked when $P_{after ori-fice}/P_t$ < 0.528 for a diatomic gas (γ = 1.4) . From Table 1, it is seen that the orifice choked when the console pressure was between - 2.5 and 0 psig.

The flow tube in the MFM is 0.056 inches in diameter and 17.72 inches (45 cm) long. Since the other flow tubes in the system are 0.25 inches in diameter, it was possible that the MFM might be choked due to friction. To investigate this possibility, the pressure drop across the MFM was measured.
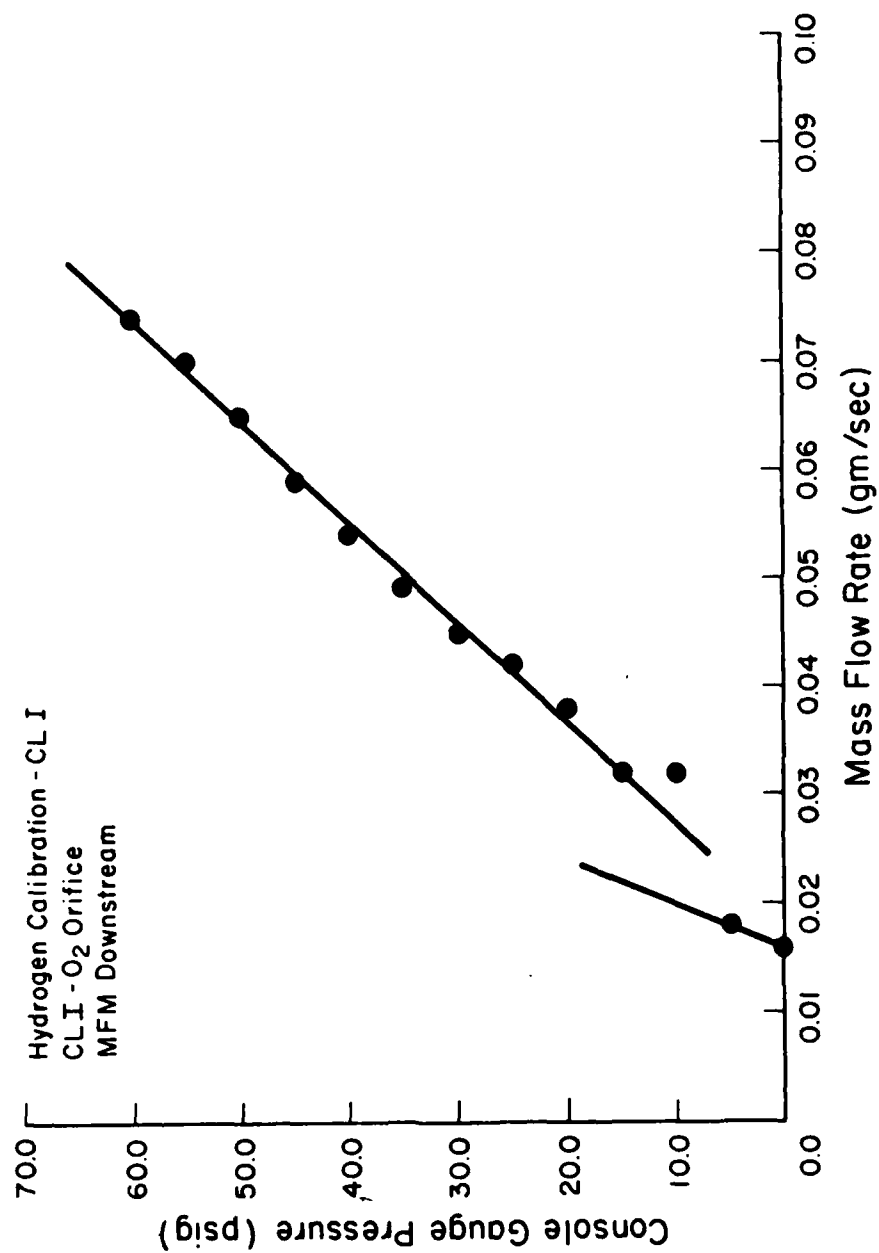
18

Figure 10. Console pressure versus H_2 mass flow rate for the CL I, for the CL I O_2 orifice, with the MFM downstream of the flow control orifice.
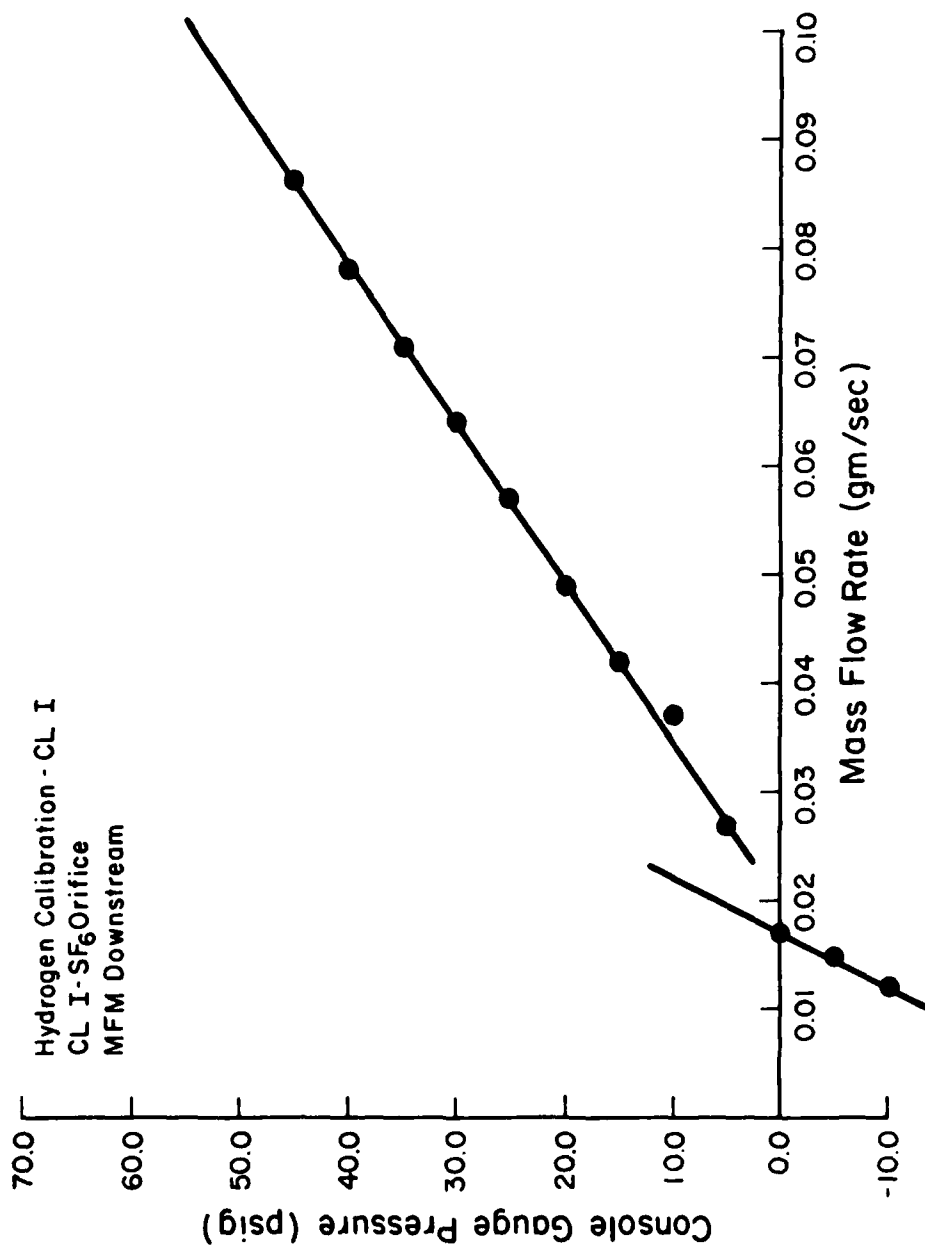
19

Figure 11. Console pressure versus H_2 mass flow rate for the CL I, for the CL I SF_6 orifice, with the MFM downstream of the flow control orifice.
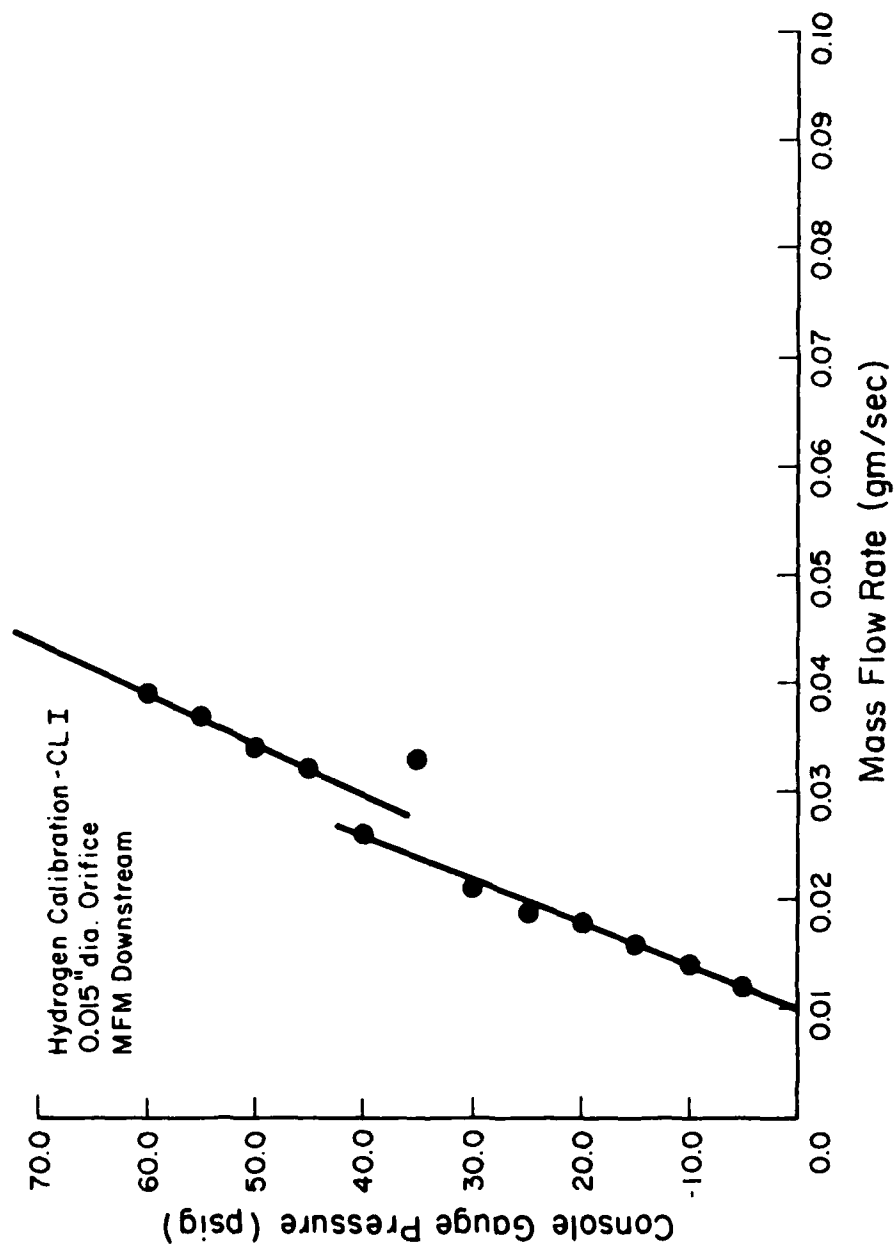
Figure 12. Console pressure versus H_2 mass flow rate for the CL I, for the 0.015 inch diameter orifice, with the MFM downstream of the flow control orifice.

H_2 CONSOLE PRESSURE (PSIG)	H_2 CONSOLE PRESSURE (PSIA)	H_2 MASS FLOW RATE (gm/sec)	PRESSURE AFTER ORIF. (PSIA)	P_{AFTER} ORIFICE$/P_t$
-9.8	4.89	0.0	4.14	0.849
-7.37	7.32	0.0	4.87	0.665
-4.9	9.79	0.0	5.46	0.558
-2.46	12.23	0.0	6.59	0.539
0	14.69	0.0	7.23	0.492
5	19.69	0.013	8.31	0.422
10	24.69	0.015	9.29	0.376
15	29.69	0.016	10.28	0.346
20	34.69	0.017	11.26	0.324
25	39.69	0.024	12.24	0.308
30	44.69	0.027	13.47	0.301
35	49.69	0.032	14.69	0.296
40	54.69	0.035	15.94	0.291
45	59.69	0.038	17.19	0.288
50	64.69	0.041	17.94	0.277
55	69.69	0.043	18.89	0.271
60	74.69	0.044	19.89	0.266

Table 1: Pressure drop across orifice #1 as a function of console pressure when the mass flow meter was downstream of the orifice.

The geometry of the pressure drop measurement is shown in Fig. 13. The data are presented in Table 2. To determine whether the measured pressure drop was sufficient to choke the MFM, a calculation of the pressure drop assuming the MFM was choked was made. It was assumed that the flow between point 1, where the upstream pressure was measured, and the inlet to the MFM point I, and the flow between the exit of the MFM point e and point 2, where the downstream pressure was measured, were isentropic, i.e., $P_{t_I} = P_{t_1}$ and $P_{t_e} = P_{t_2}$. Since the ratio of the areas of 1 and I and e and 2 was 20, $M_1 \simeq 0$ and $M_2 \approx 0$ and thus, $P_1 \approx P_{t_1}$ and $P_2 \approx P_{t_2}$. With the assumption of quasi-one-dimensional flow through the MFM, the pressure drop was calculated as follows. The measured mass flow rate $\dot{m}$ was used to calculate the Reynolds number

$$Re = \frac{2\dot{m}}{\pi R \mu} \tag{3.1-1}$$

With the Reynolds number, the friction factor f was calculated from the relations

$$f = 16\ Re^{-1} \qquad Re < 2300 \tag{3.1-2}[3]$$

$$f = (23025.1)^{-1}\ Re^{0.6558} \qquad 2300 < Re < 4000 \tag{3.1-3}[4]$$

$$f = (0.3164/4)\ Re^{-0.25} \qquad Re > 4000 \tag{3.1-4}[5]$$

With f known and with the assumption that the pipe is choked ($M_e = 1$),

$$\frac{4fL}{D} = \frac{4fL_{MAX}}{D} \tag{3.1-5}$$

can be used to calculate M_I, the inlet Mach number. With the inlet Mach number, $P_{t_I}/\tilde{P}_t = P_{t_I}/P_{t_e} = P_{t_1}/P_{t_2} = P_1/P_2$ is obtained from the Tables for Fanno flow[2]. The results of these calculations are given in Table 3. Comparison of the measured and calculated pressure ratios across the MFM shows
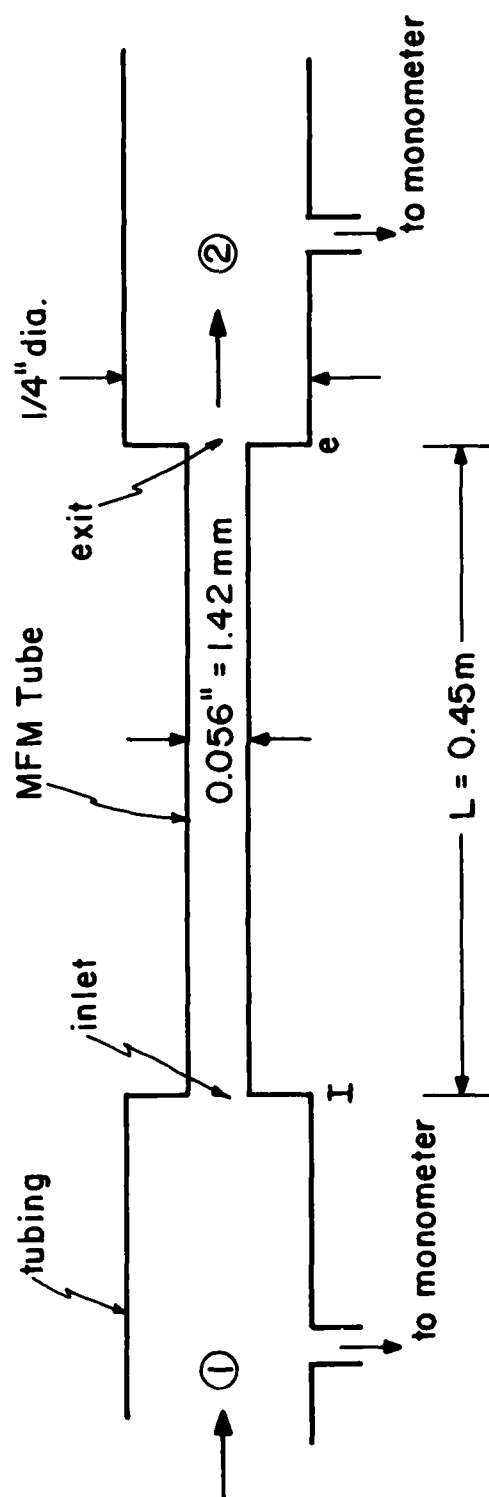
Figure 13. A schematic of the experimental measurement of the pressure drop across the mass flow meter.

H$_2$ CONSOLE PRESSURE (PSIG)	H$_2$ MASS FLOW RATE (gm/sec)	PRESSURE BEFORE MFM P$_1$ (PSIA)	PRESSURE AFTER MFM P$_2$ (PSIA)	ΔP ACROSS MFM (PSI)	$\frac{P_2}{P_1}$
-9.8	0.0	1.89	0.58	1.31	0.3069
-7.37	0.0	2.88	0.89	1.99	0.3090
-4.9	0.0	3.60	1.09	2.52	0.3027
-2.46	0.0	4.27	1.27	3.00	0.2974
0	0.012	4.83	1.43	3.40	0.2961
5	0.014	5.96	1.73	4.23	0.2903
10	0.016	7.09	2.03	5.05	0.2863
15	0.018	8.13	2.31	5.82	0.2841
20	0.019	9.12	2.58	6.54	0.2825
25	0.026	10.09	2.84	7.25	0.2815
30	0.027	11.11	3.10	8.01	0.2790
35	0.033	12.26	3.32	8.94	0.2708
40	0.036	13.31	3.52	9.78	0.2645
45	0.040	14.49	3.78	10.71	0.2609

Table 2: Pressure drop across the MFM as a function of console pressure when the mass flow meter was downstream of the orifice.

$P_{console}$ (psig)	$\dot{m}_{exp}$ (gm/sec)	Re	$\dfrac{4fL}{D}$	M_I	$\dfrac{P_{t_e}}{P_{t_I}} = \dfrac{P_{t2}}{P_{t1}} = \dfrac{P_2}{P_1}$
0	0.014	1570	12.92	0.2096	0.3531
5	0.016	1790	11.30	0.2217	0.3723
10	0.019	2130	9.52	0.2379	0.3978
15	0.022	2240	9.05	0.2429	0.4056
20	0.024	2690	9.77	0.2354	0.3939
25	0.030	3360	11.31	0.2216	0.3723
30	0.035	3925	12.51	0.2125	0.3577
35	0.036	4035	12.58	0.2120	0.3570
40	0.040	4480	12.25	0.2144	0.3608
45	0.043	4820	12.03	0.2160	0.3633

Table 3. Calculated pressure drop across the MFM.

that the measured pressure drop was always greater than the value calculated assuming the MFM was choked. This indicates that the MFM was choked.

These calculations also indicate that the Reynolds number of the flow in the MFM reaches the critical value of 2300 for console pressures between 15 and 20 psig, which is about where the break in the slope of the console pressure versus mass flow curve occurs. This suggests that when the flow in the mass flow meter switches from laminar to turbulent, the controlling element in the flow system switches from the mass flow meter to the flow control orifice. The reasons for this behavior are not completely understood.

To circumvent the MFM control of the flow rate for console pressures below 20 psig, the MFM was inserted into the H_2 line at position A upstream of the flow control orifice, Fig. 1. In this case, the pressure drop across the MFM was measured to be less than 1 psi for all flow rates. Thus, the MFM did not choke. The mass flow data for orifice #1 are shown in Fig. 14. Again a break is observed in the slope of the P_c versus $\dot{m}$ curve for values of P_c between 20 and 25 psig for a mass flow rate of about 0.030 gm/sec. In this case, the upper slope increased whereas with the MFM downstream of the orifice, the upper slope decreased with respect to the lower slope. This change in slope indicates that the controlling area decreased as the mass flow rate passed through 0.030 gm/sec.

Measurement of the pressure drop across the orifice showed that the orifice was choked for all values of $P_c > -1.9$ psig. For a choked orifice, Eq. (2.1-2) can be differentiated to obtain

$$\frac{dP_t}{d\dot{m}} = \sqrt{\frac{RT_t}{\gamma}} \left(\frac{\gamma+1}{2}\right)^{\frac{\gamma+1}{2(\gamma-1)}} \frac{1}{A_e} \qquad (3.1\text{-}6)$$
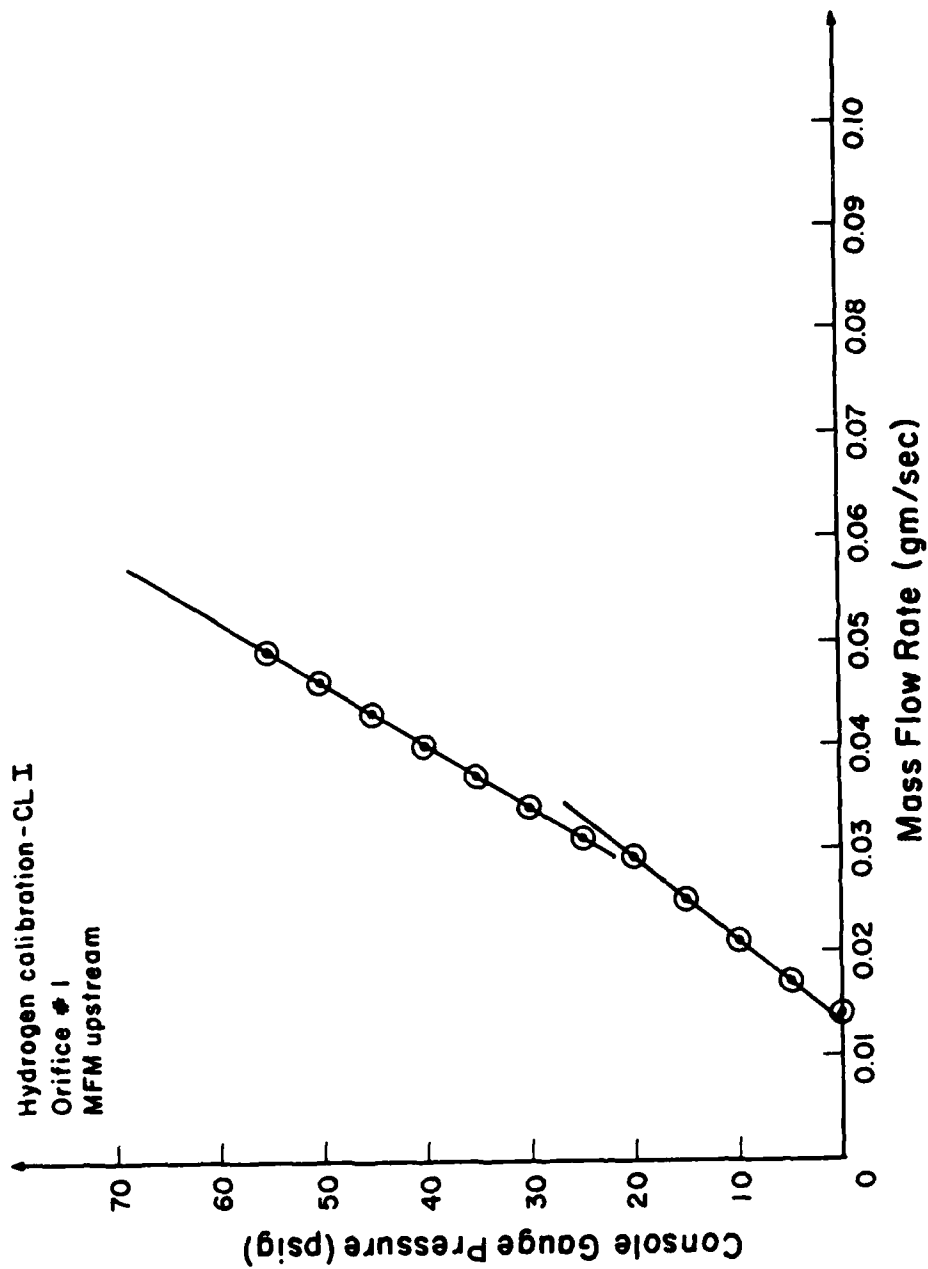
Figure 14. Console pressure versus H_2 mass flow rate for the CL I, for orifice #1, with the MFM upstream of the flow control orifice.

From the measured slope of the P_t versus $\dot{m}$ curve, the size of the controlling area can be determined. Since the flow rates are small, the flow upstream of the orifice can be assumed isentropic with the total temperature equal to 300°K. With these assumptions, the areas deduced from the lower and upper slopes of Fig. 14 are compared to the orifice area in Table 4. From this table, it is seen that the upper slope agrees with the geometric orifice area (within 5.8%) while the lower slope corresponds to an area that is 21% greater than the orifice area. This suggests a change in the effective size of the orifice occurs at the break in the slope of the P_c versus $\dot{m}$ curve. Such a change could be caused by a change in the thickness of the boundary layer in the orifice.

To investigate this possibility, a simple model of the orifice flow was considered. The orifice flow field was divided into two regions, a uniform potential core and a boundary layer, Fig. 15. For the type of orifices used (L/D ~ 2), the velocity profile was not fully developed[6]. The thickness of the boundary layer was assumed to have the same functional dependence as a flat plate boundary layer. However, since the Reynolds number at which the transition from laminar to turbulent flow occurs is not known for the orifice, it was assumed to occur at the Reynolds number at which the break in the slope of the P_c versus $\dot{m}$ curve occurs. With these assumptions, the mass flow rate through the orifice exit plane can be calculated by summing the mass flow through the boundary layer region and the mass flow through the core region, i.e.,

$$\dot{m}_{core} = \rho_{core} \, U_{core} \, A_{core} \tag{3.1-7}$$

$$\dot{m}_{BL} = \int_{R-\delta}^{R} \rho U_z(r) \, 2\pi r dr \tag{3.1-8}$$

$$\dot{m} = \dot{m}_{core} + \dot{m}_{BL} \tag{3.1-9}$$

A_{upper}	$1.461 \times 10^{-7} m^2$	D_{upper}	0.01698 in
A_{lower}	$1.884 \times 10^{-7} m^2$	D_{lower}	0.0193 in
$A_{orifice \#1}$	$1.551 \times 10^{-7} m^2$	$D_{orifice \#1}$	0.0175 in

Table 4. Comparison of the orifice area with the effective areas deduced from the upper and the lower slopes of the P_c versus $\dot{m}$ curve of Fig. 14.
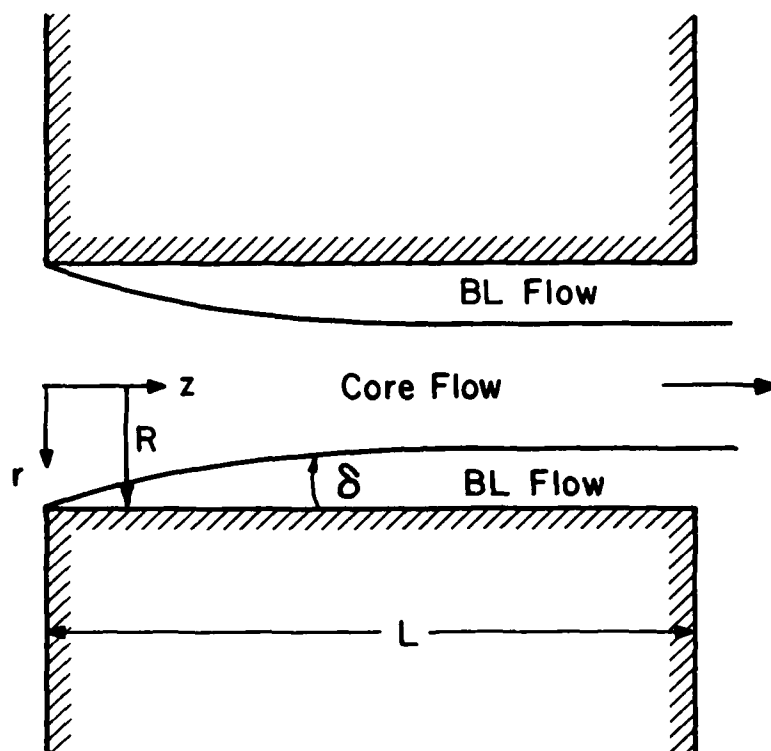
Figure 15. A schematic diagram of the orifice and the coordinate system for the orifice flow model.

With the usual assumptions for axisymmetric, steady, incompressible pipe flow, the Navier-Stokes equations reduce to

$$0 = \frac{1}{r} \frac{d}{dr} \left(r \, \mu \, \frac{dU_z}{dr} \right) \qquad (3.1-10)$$

with the boundary conditions

$$at \quad r = R \qquad , \qquad U_z = 0$$
$$(3.1-11)$$
$$at \quad r = R-\delta \qquad , \qquad U_z = U_{core}$$

The solution of Eq. (3.1-10) that satisfies the boundary conditions (3.1-11) is

$$U_z = U_{core} \frac{\ell n(r/R)}{\ell n[(R-\delta) \, / \, R]} \qquad for \quad R-\delta < r < R \qquad (3.1-12)$$

Substitution of Eq. (3.1-12) into Eq. (3.1-8) gives

$$\dot{m}_{BL} = \frac{2\pi\rho_{core}U_{core}}{\ell n\left(\frac{R-\delta}{R}\right)} \left[\frac{(R-\delta)^2 - R^2}{4} - \frac{(R-\delta)^2}{2} \ell n\left(\frac{R-\delta}{R}\right) \right] \qquad (3.1-13)$$

The total mass flow rate is then given by

$$\dot{m} = \rho_{core} \, U_{core} \, A_{core} \frac{\left[1 - \left(\frac{R}{R-\delta}\right)^2 \right]}{\ell n\left[\frac{R-\delta}{R}\right]^2} \qquad (3.1-14)$$

Since the core flow is inviscid, isentropic and choked at the orifice exit,

$$\rho_{core}U_{core}A_{core} = \sqrt{\frac{\gamma}{RT_t}} \, P_t \, \left(\frac{2}{\gamma+1}\right)^{\frac{\gamma+1}{2(\gamma-1)}} \pi(R-\delta)^2 \qquad (3.1-15)$$

With the assumption that a transition from laminar to turbulent flow occurs at the Reynolds number corresponding to the break in the slope of the P_c versus $\dot{m}$ curve, the boundary layer thickness is assumed to be given by the flat plate results[7]

$$\frac{\delta}{L} = \frac{5}{\sqrt{Re}} \qquad \text{for} \quad Re < Re_{critical} \qquad (3.1\text{-}16)$$

and

$$\frac{\delta}{L} = \frac{0.35}{(Re)^{1/5}} \qquad \text{for} \quad Re_{critical} < Re \qquad (3.1\text{-}17)$$

where the Reynolds number is calculated by

$$Re = \frac{\rho_{core} U_{core} L}{\mu} = \frac{L}{\mu} P_t \sqrt{\frac{\gamma}{RT_t}} \left(\frac{2}{\gamma+1}\right)^{\frac{\gamma+1}{2(\gamma-1)}} \qquad (3.1\text{-}18)$$

and L is the thickness of the orifice. The console pressure P_c was assumed to be P_t for the orifice and the total temperature was taken to be 300°K. The results of this model are shown in Fig. 16 for an orifice shaped like #2, Fig. 8. From Figure 16, it is seen that the break in the P_c versus $\dot{m}$ curve shifts the upper slope in the same direction as the data. This result supports the hypothesis that the break is the result of a transition from laminar to turbulent flow in the orifice. Since the turbulent boundary layer is thicker than the laminar boundary layer, the effective flow area in the laminar case would be larger than in the turbulent case. This agrees with the fact that the effective area calculated from the slope of the lower curve is larger than the effective area calculated from the slope of the upper curve.

Since the break in the P_c versus $\dot{m}$ curves appeared to be the result of a laminar to turbulent flow transition, this boundary layer effect should be minimized if thin orifices are used. To determine the validity of this
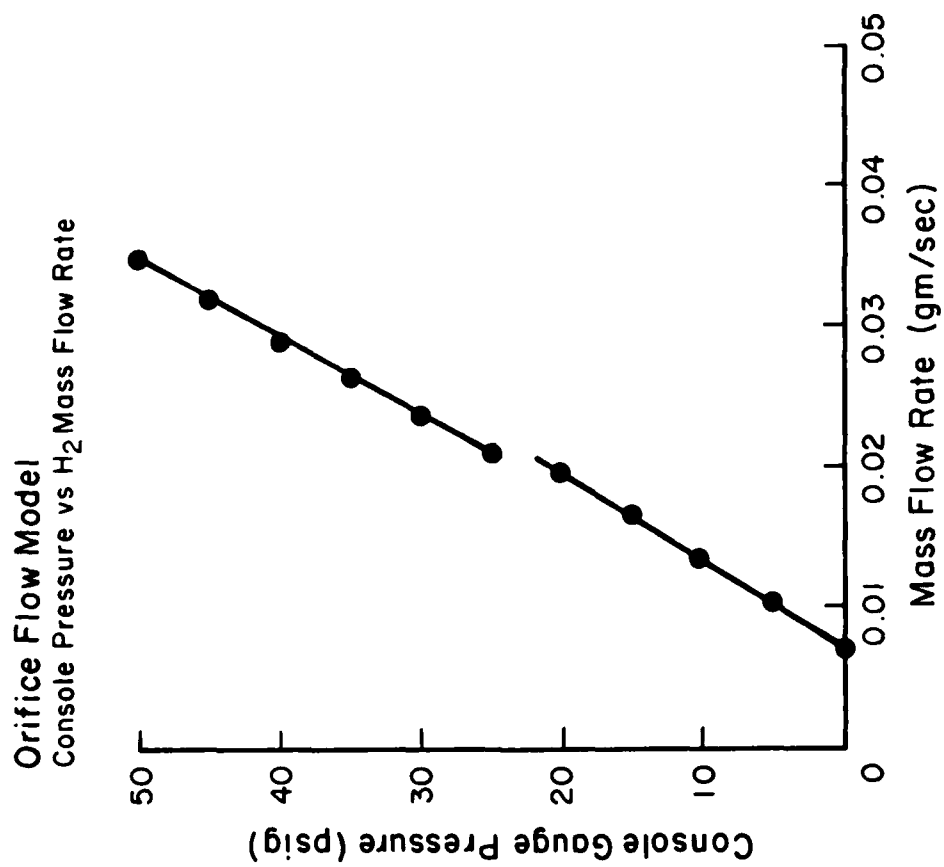
Orifice Flow Model
Console Pressure vs H_2 Mass Flow Rate

Console Gauge Pressure (psig)

Mass Flow Rate (gm/sec)

Figure 16. Console pressure versus H_2 mass flow rate as calculated by the orifice flow model.

hypothesis, the experiments were repeated with two different thin orifices, #3 and #4, Fig. 8. The resulting data are shown in Figs. 17 and 18. From these figures, it is seen that the break in slope does not occur. The difference in the slopes of these curves is due to the difference in the areas of the two orifices. Orifice #4 was chosen for use in the CL I laser control console.

From the theory of the choked orifice, the extrapolation of the P_c versus $\dot{m}$ straight line to zero absolute console pressure should give zero mass flow rate, Fig. 2. It was found that whether the measured P_c versus $\dot{m}$ curves extrapolated to zero mass flow at zero absolute P_c depended upon the adjustment of the zero point of the mass flow meter. Compared to the values of $\dot{m}$ to be measured, the zero point of the MFM has a relatively large error associated with it. However, the slope of the P_c versus $\dot{m}$ data was found to be independent of the zero point setting of the MFM. This is illustrated in Figs. 19 and 20, which show P_c versus $\dot{m}$ data for two different adjustments of the zero point of the MFM for orifice #4. Since the slope of P_c versus $\dot{m}$ is independent of the zero point setting of the MFM, the data can be corrected for errors in the zero point setting by shifting the data horizontally on the P_c versus $\dot{m}$ plot until the extrapolated straight line intersects the origin ($\dot{m} = 0$ at $P_c = 0$ psia). This correction has been applied to all the mass flow calibration data. The resulting CL I H_2 mass flow calibration curve is shown in Fig. 21.

3.2 CL I SF_6, O_2 and He Calibration

The MFM was inserted into the flow system for each of the other input species upstream of the flow control orifice at point A, Fig. 1. The resulting console pressure versus mass flow rate curves are given in Figs. 22-24. All of these data fell on straight lines as expected.
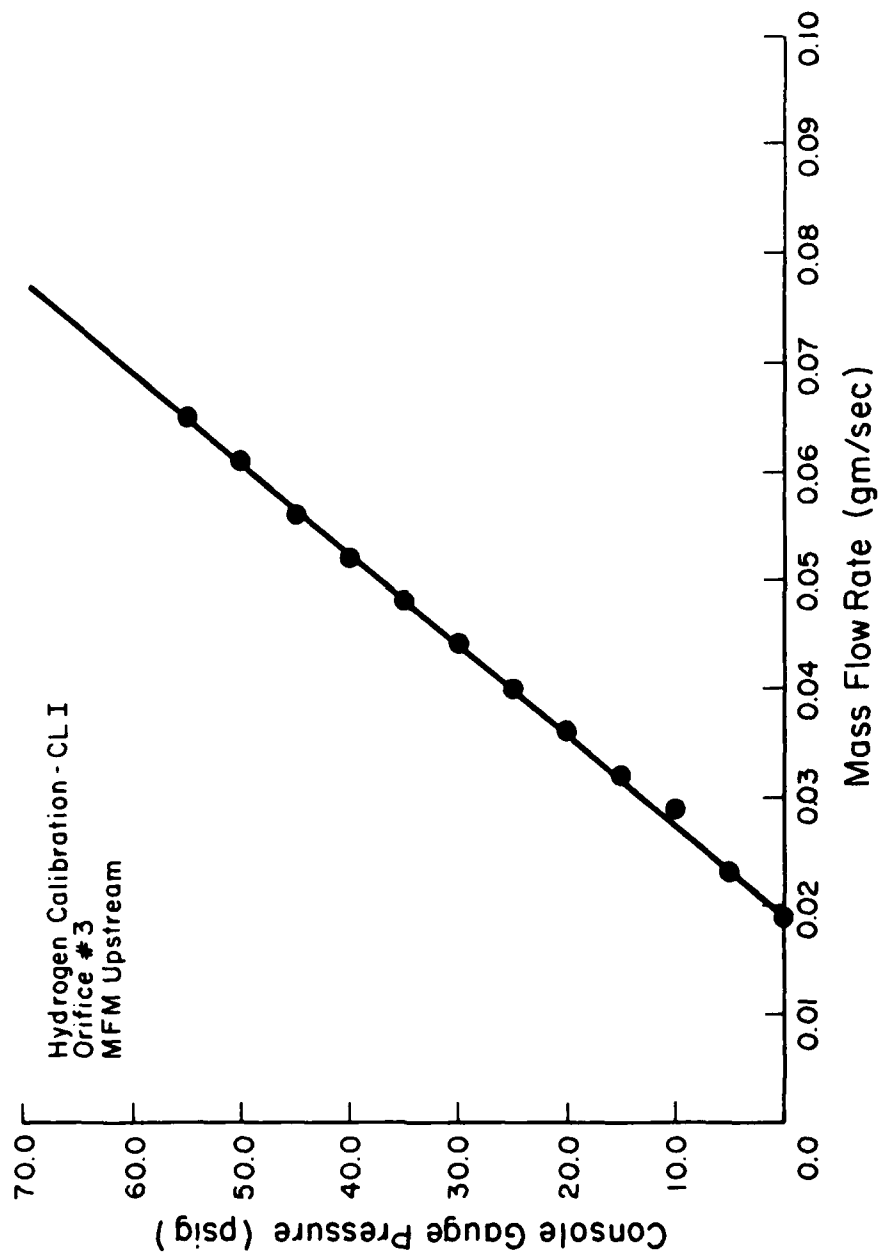
Figure 17. Console pressure versus H_2 mass flow rate for the CL I, for orifice #3, with the MFM upstream of the flow control orifice.
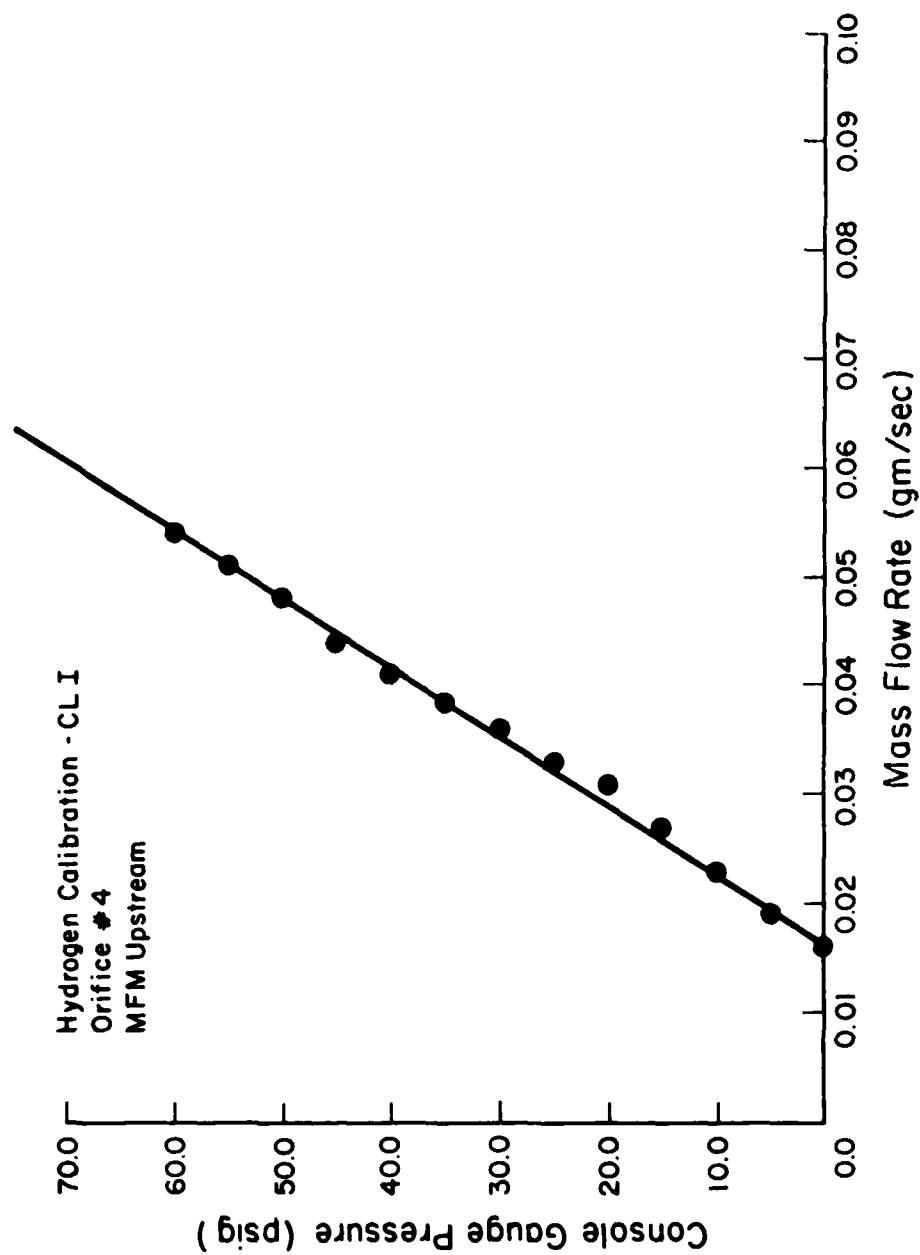
Figure 18. Console pressure versus H_2 mass flow rate for the CL I, for orifice #4, with the MFM upstream of the flow control orifice.
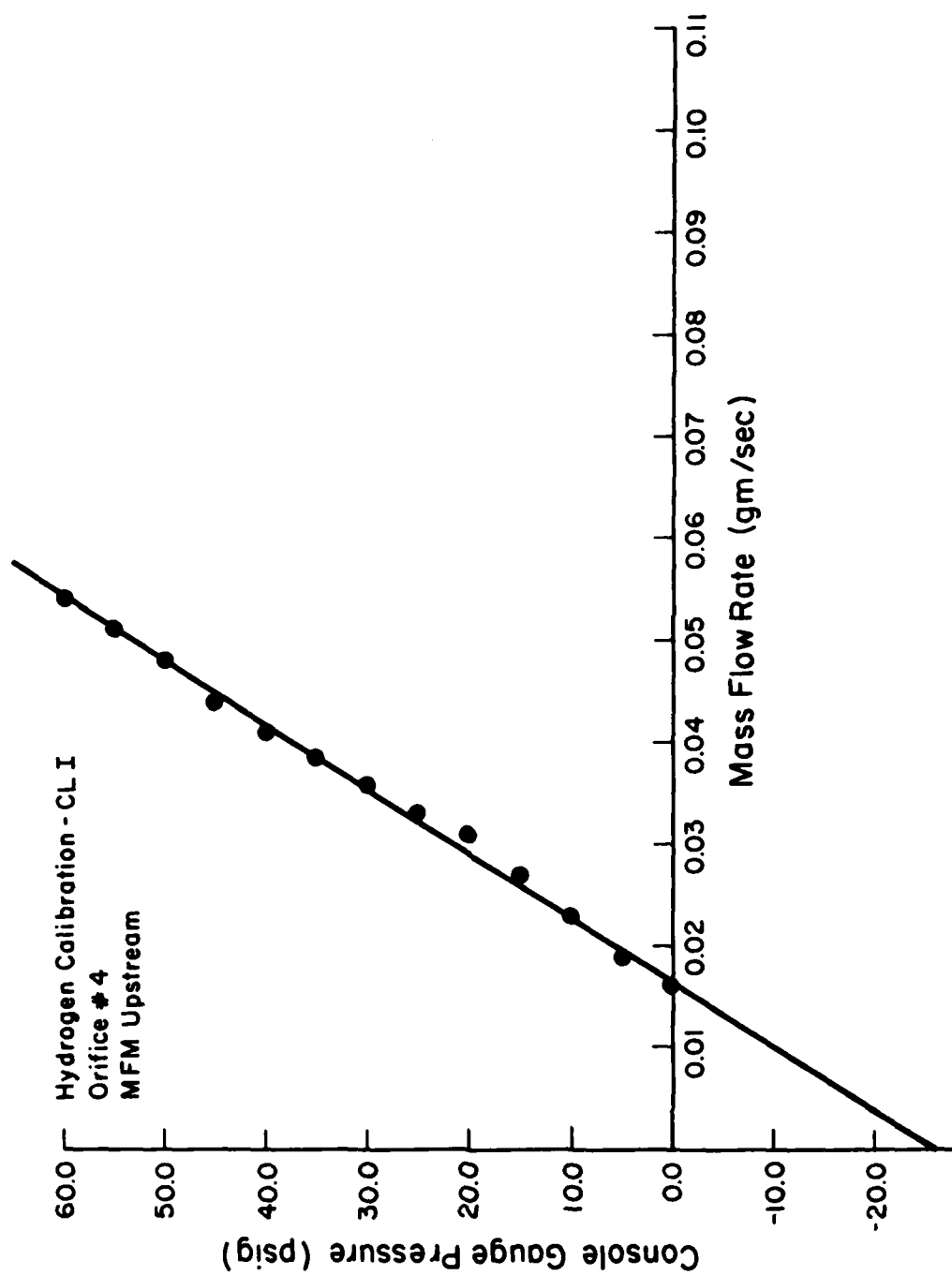
Figure 19. Console pressure versus H_2 mass flow rate for the CL I, for orifice #4, with the MFM upstream of the flow control orifice, showing the extrapolation to zero mass flow rate.
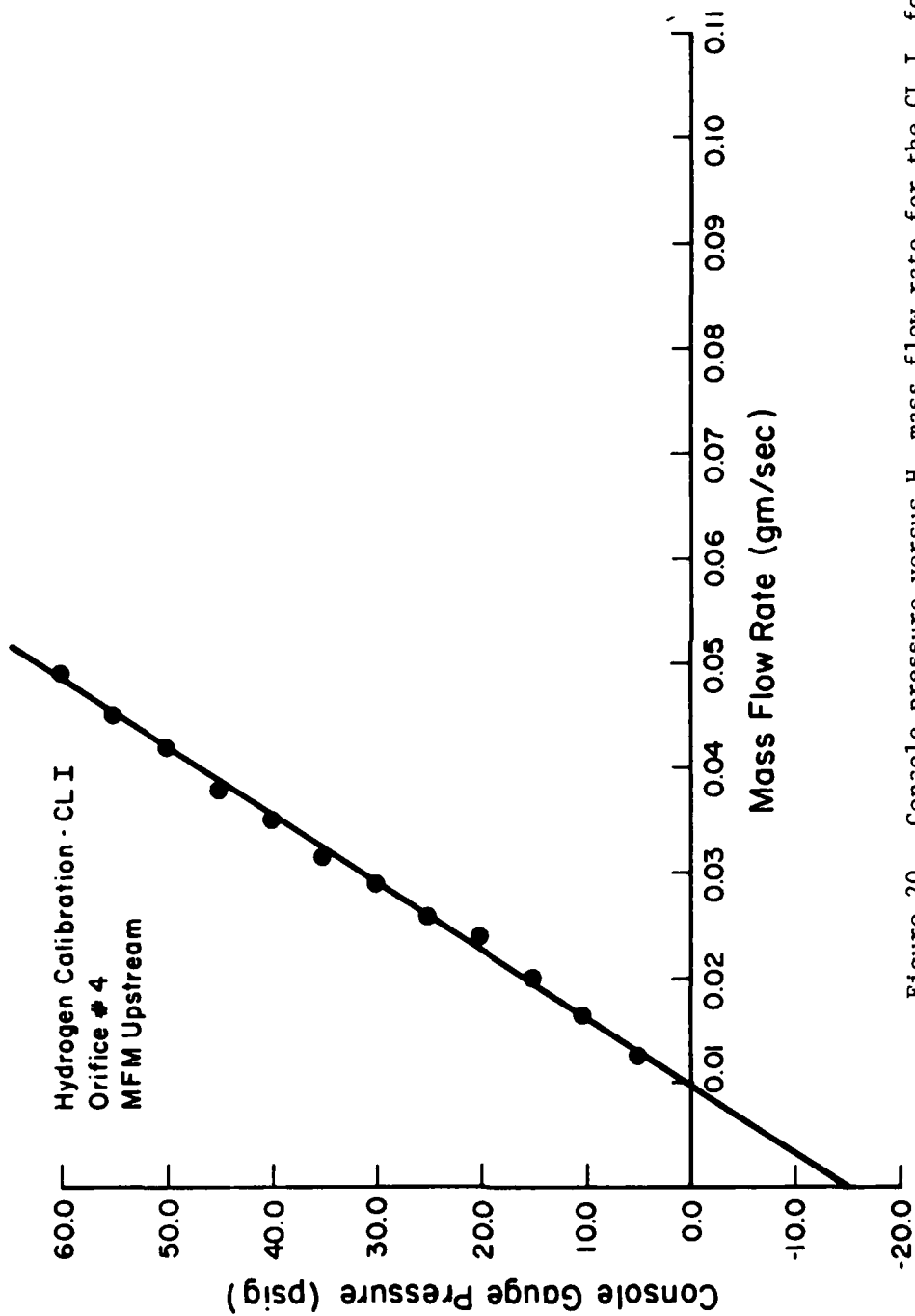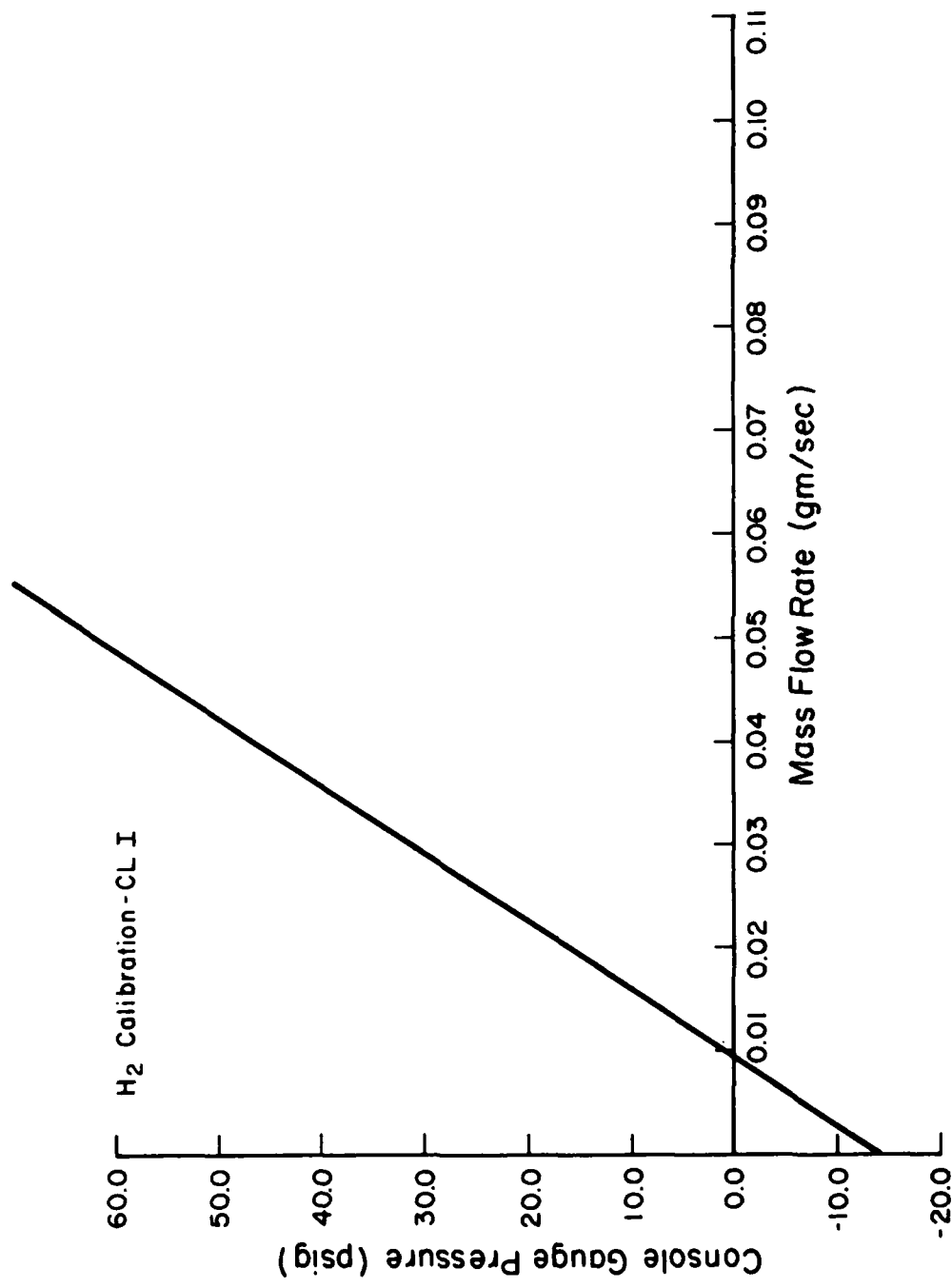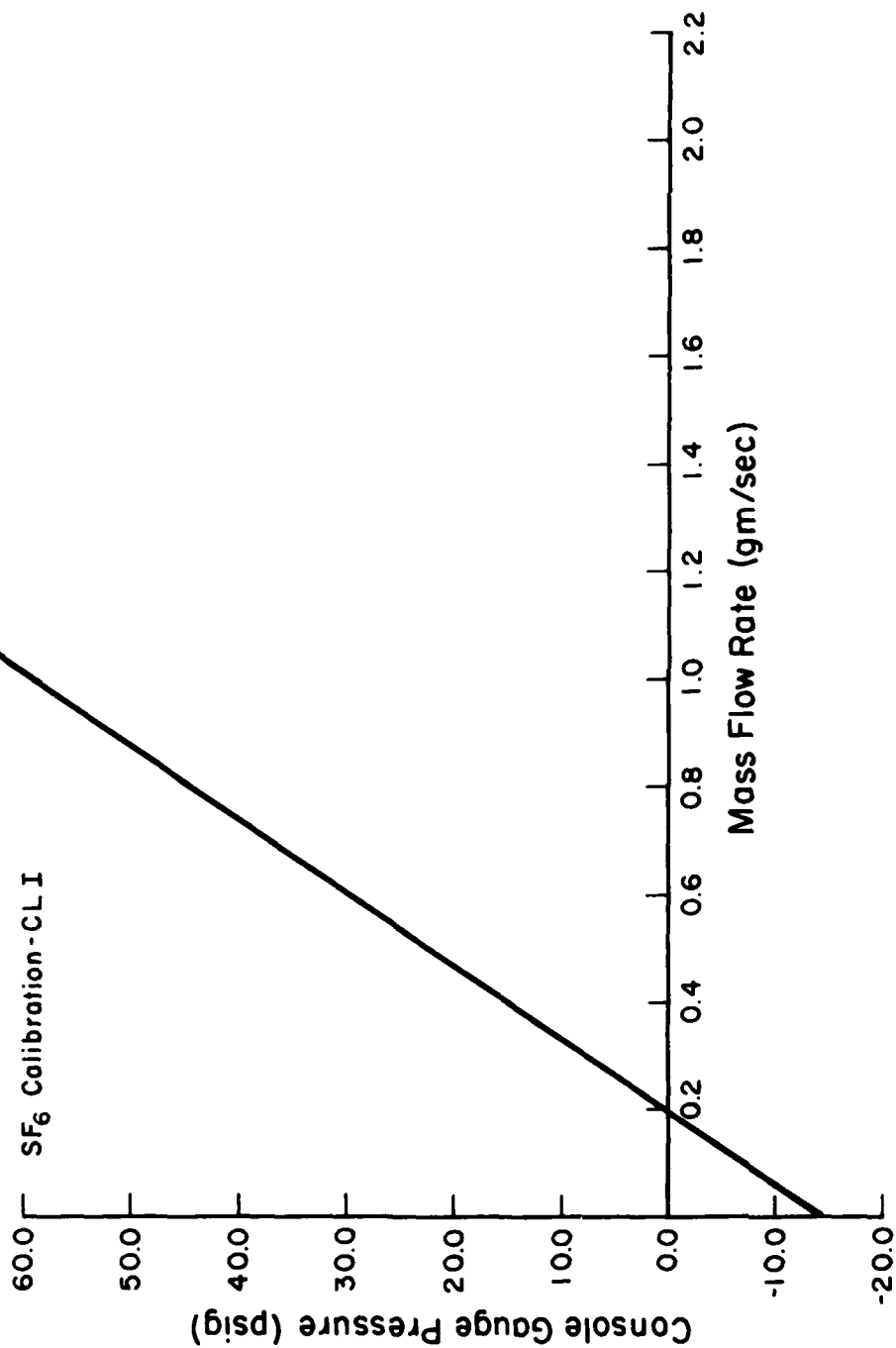
Figure 20. Console pressure versus H_2 mass flow rate for the CL I, for orifice #4, with the MFM upstream of the flow control orifice, showing the extrapolation to zero mass flow rate for a slightly different setting of the zero point of the MFM.

39

Figure 21. Console pressure versus H_2 mass flow rate for the CL I, for orifice #4, with the MFM upstream of the flow control orifice, corrected to extrapolate to zero mass flow rate at zero psia.
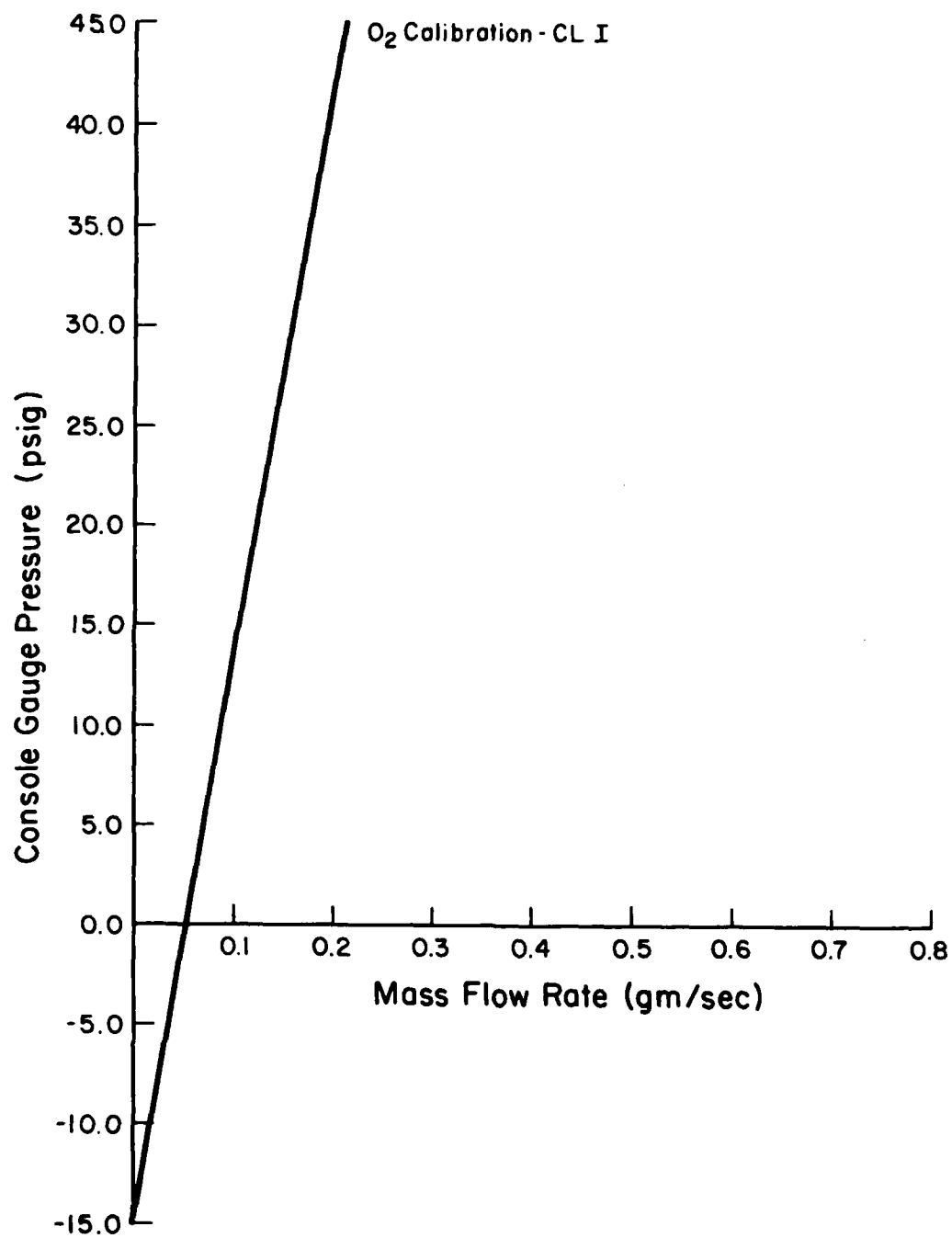
Figure 22. Console pressure versus SF$_6$ mass flow rate for the CL I, with the MFM upstream of the flow control orifice, corrected to extrapolate to zero mass flow rate at zero psia.

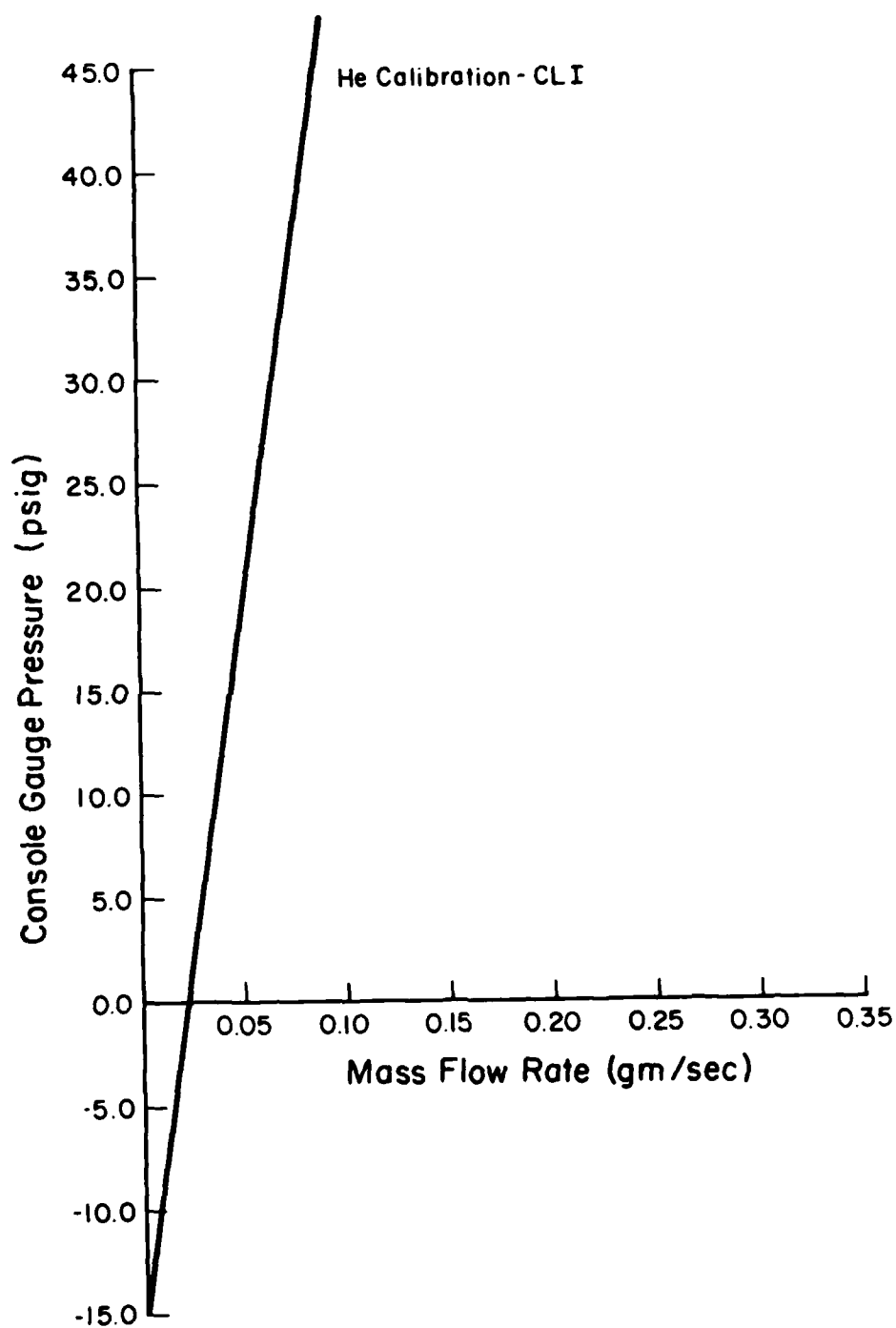Figure 23. Console pressure versus O_2 mass flow rate for the CL I with the MFM upstream of the flow control orifice, corrected to extrapolate to zero mass flow rate at zero psia.

Figure 24. Console pressure versus He mass flow rate for the CL I, with the MFM upstream of the flow control orifice, corrected to extrapolate to zero mass flow rate at zero psia.

3.3 CL II H_2, SF_6, O_2 and He Calibration

To calibrate the CL II laser control console, the MFM was inserted into the flow system upstream of the flow control orifice at point A, Fig. 1, for each input species. The resulting console pressure versus mass flow curves are given in Figs. 25-28. All of these data fell on straight lines as expected.

Originally, the CL II control console was calibrated using a blow down technique[8] in which a tank of known volume was pressurized, allowed to come to equilibrium and then the pressure-time history in the tank was recorded as the tank was allowed to exhaust through the flow control orifice until the pressure in the tank decreased a certain amount. After the gas in the tank had again reached equilibrium, the pressure and temperature were measured. From these data, the mass remaining in the tank could be calculated. From the slope of the pressure versus time curve, the instantaneous mass flow rate could be determined as a function of pressure. The mass flow meter data, which is more accurate than the data obtained from the blow-down technique, are compared to the blow-down data in Figs. 29-32. These figures show that there is agreement between the two sets of data for SF_6, O_2 and He. However, there is considerable difference between the MFM and blow-down H_2 data. Since the blow down technique is inherently less accurate than the mass flow meter, the MFM data will be used.
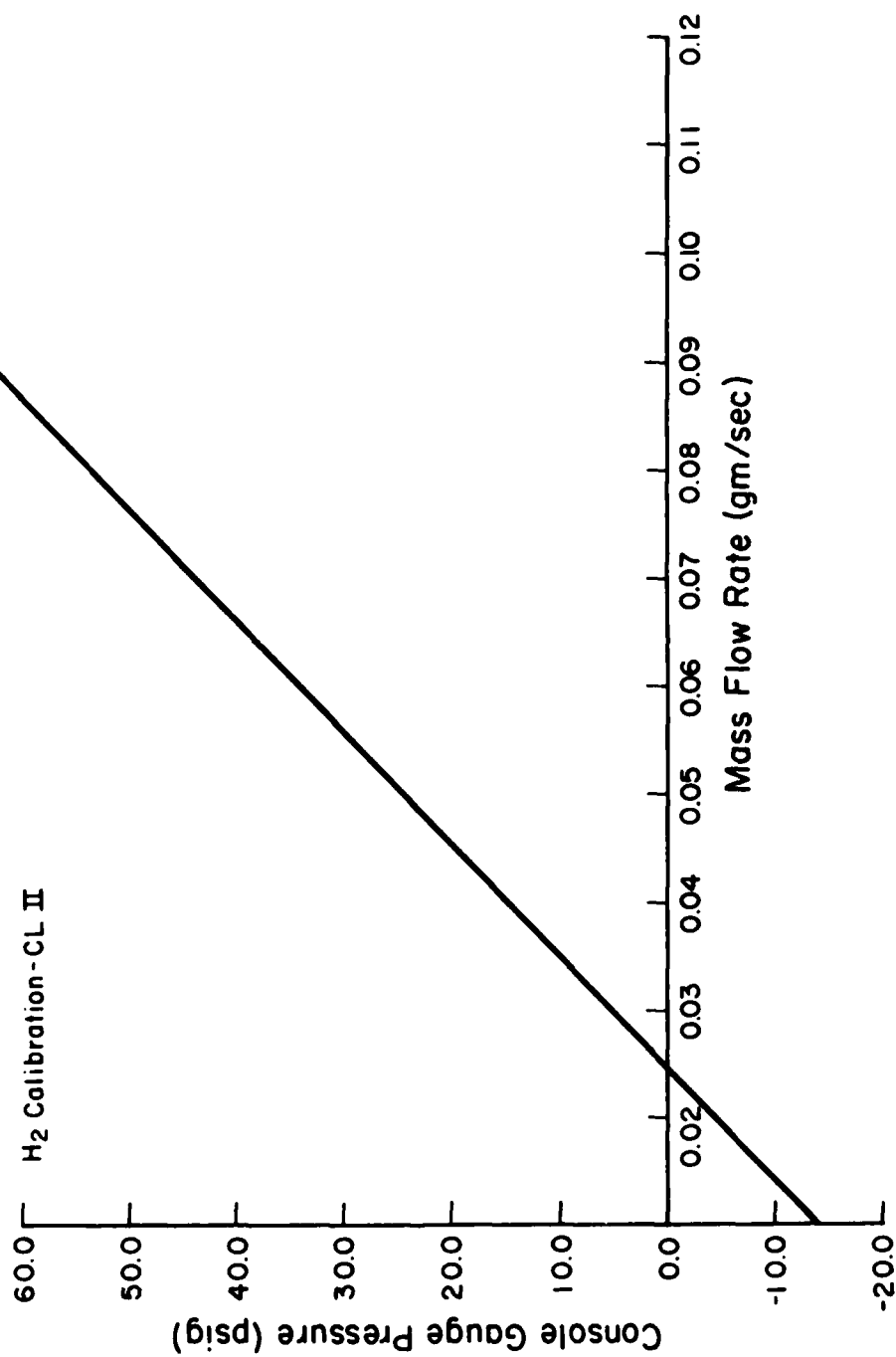
44

Figure 25. Console pressure versus H_2 mass flow rate for the CL II, with the MFM upstream of the flow control orifice, corrected to extrapolate to zero mass flow rate at zero psia.
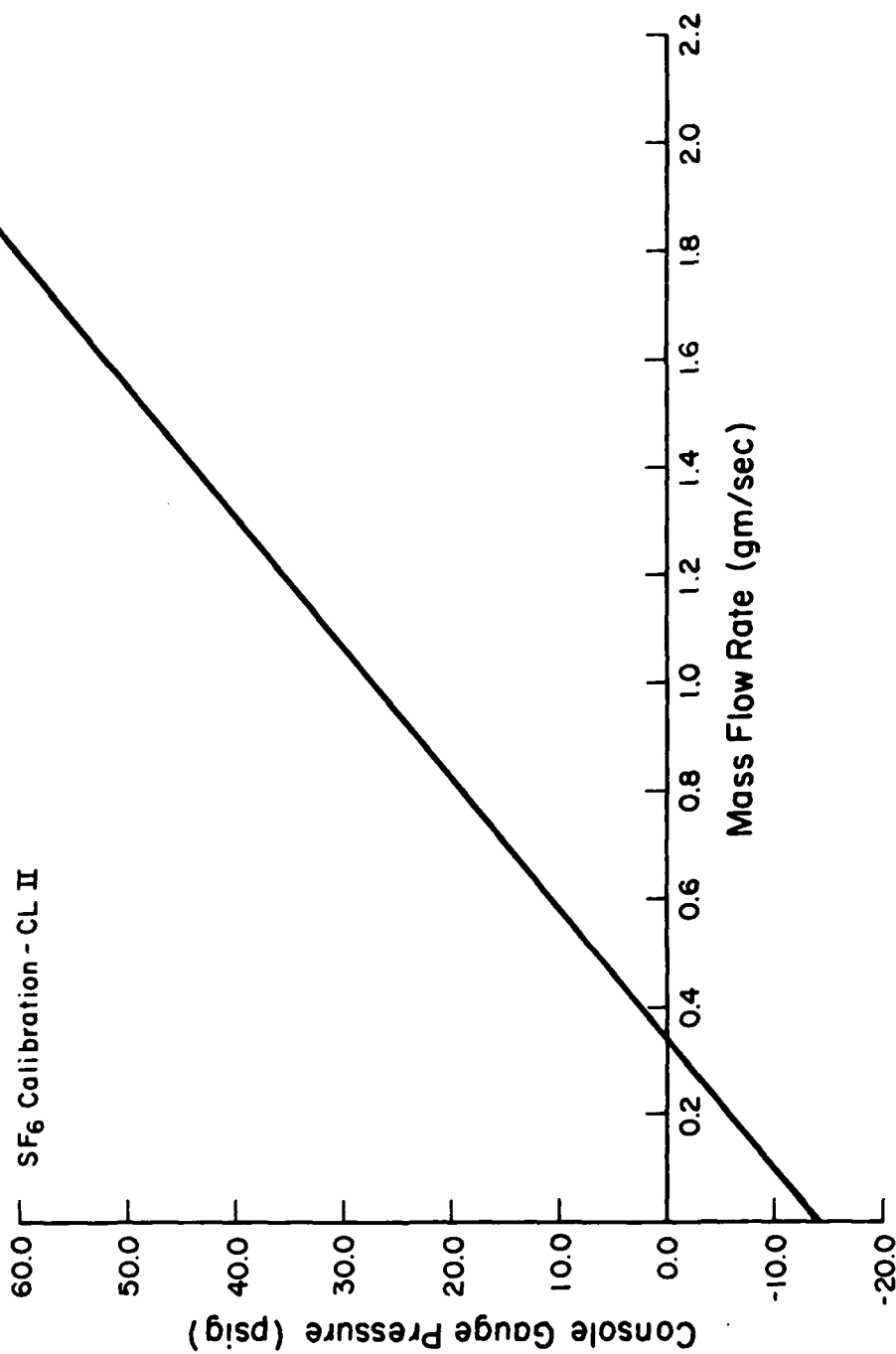
Figure 26. Console pressure versus SF_6 mass flow rate for the CL II, with the MFM upstream of the flow control orifice, corrected to extrapolate to zero mass flow rate at zero psia.
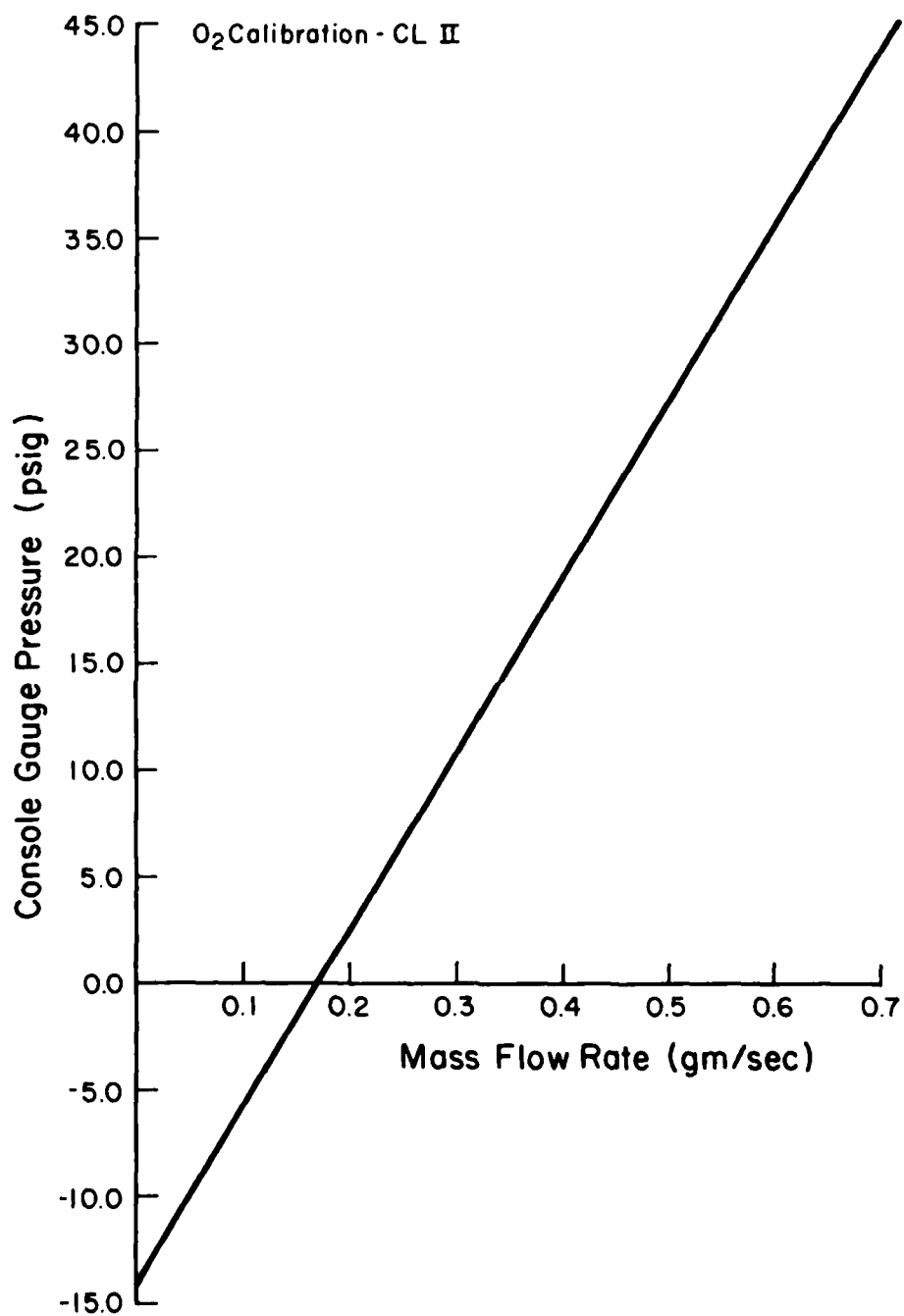
Figure 27. Console pressure versus O_2 mass flow rate for the CL II, with the MFM upstream of the flow control orifice, corrected to extrapolate to zero mass flow rate at zero psia.
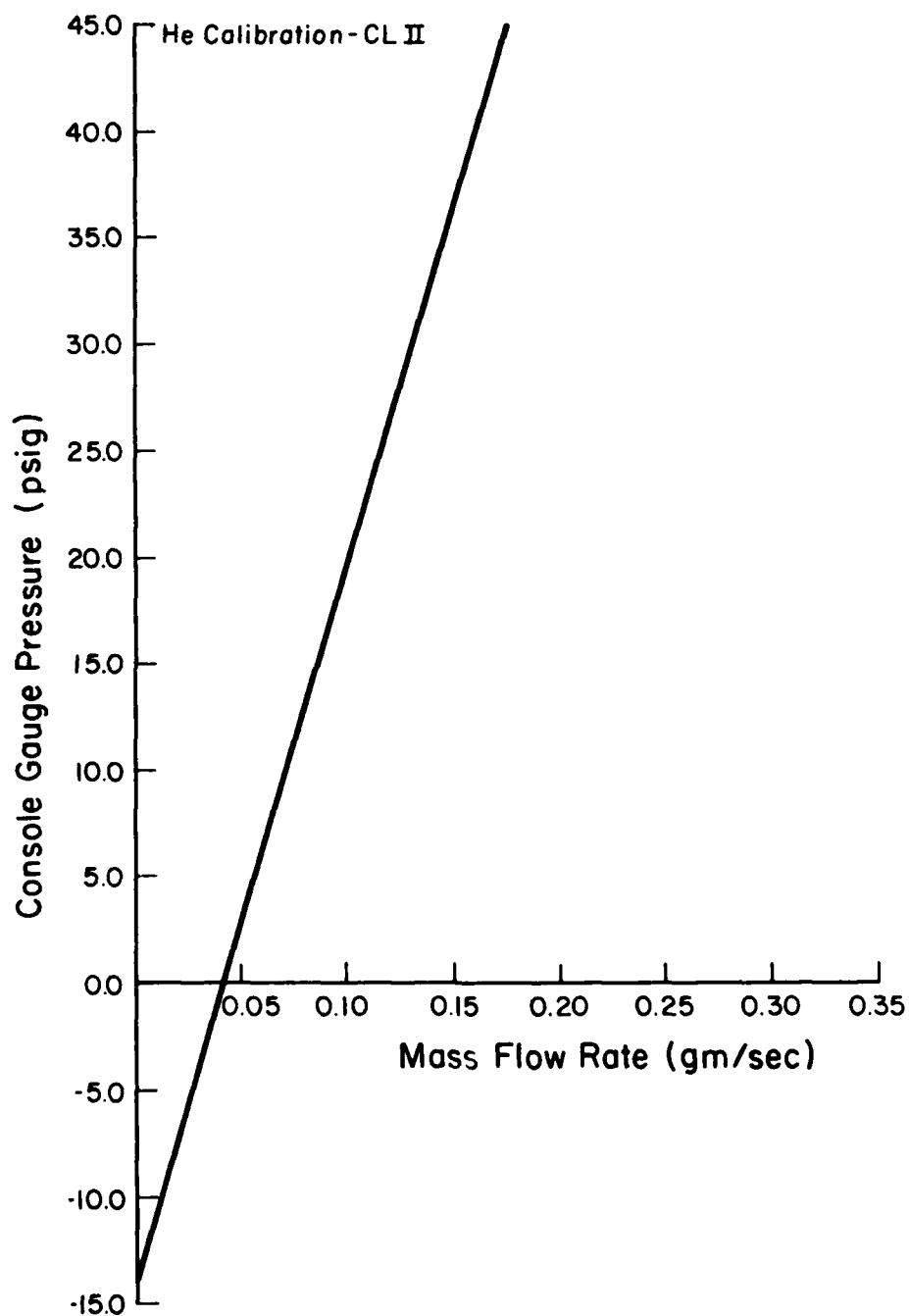
Figure 28. Console pressure versus He mass flow rate for the CL II, with the MFM upstream of the flow control orifice, corrected to extrapolate to zero mass flow rate at zero psia.
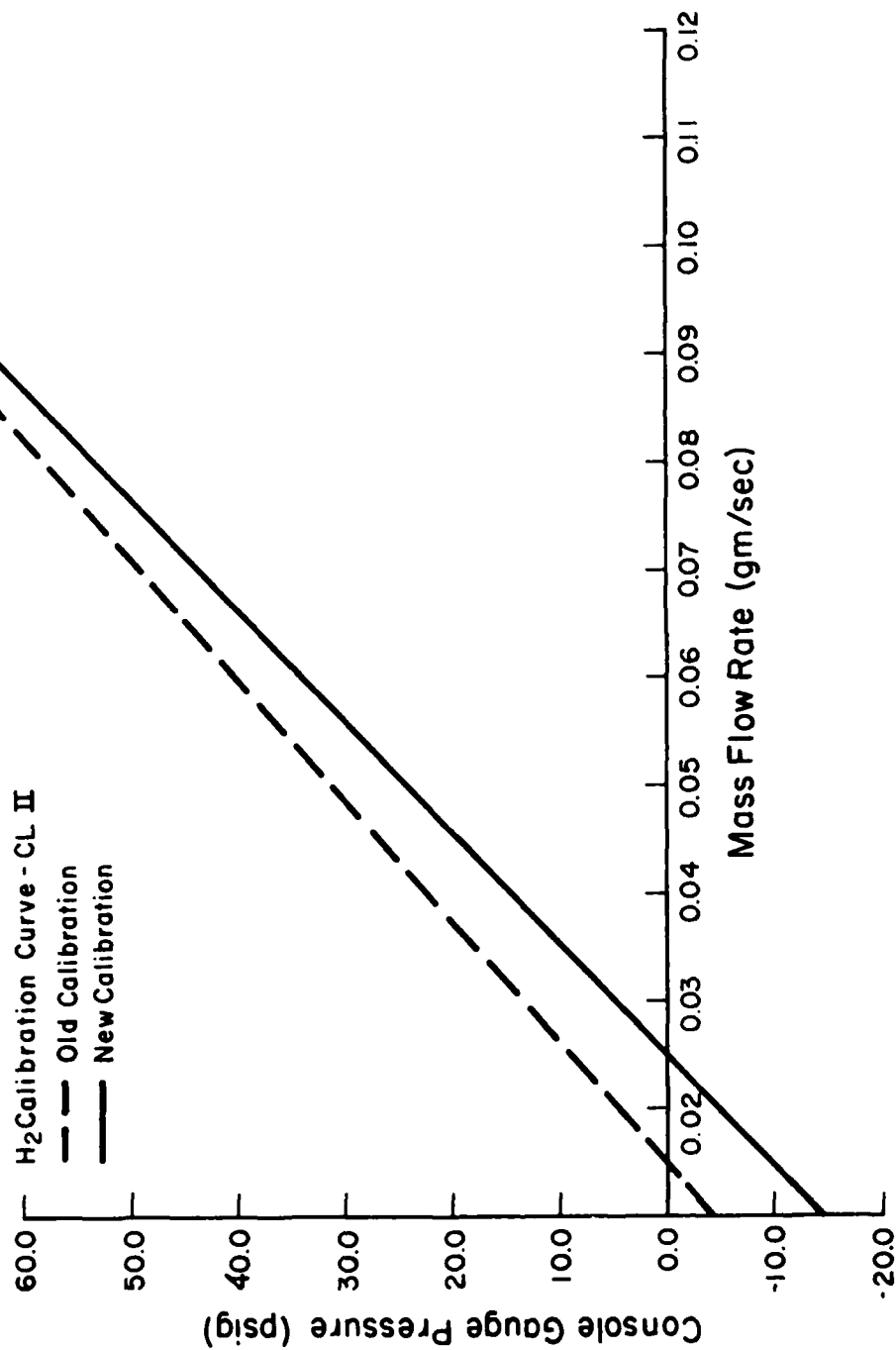
Figure 29. Comparison of the present and the original H_2 mass flow calibration curves for the CL II.

SF6 Calibration Curve CL II

— — — Old Calibration
———— New Calibration

Mass Flow Rate (gm/sec)
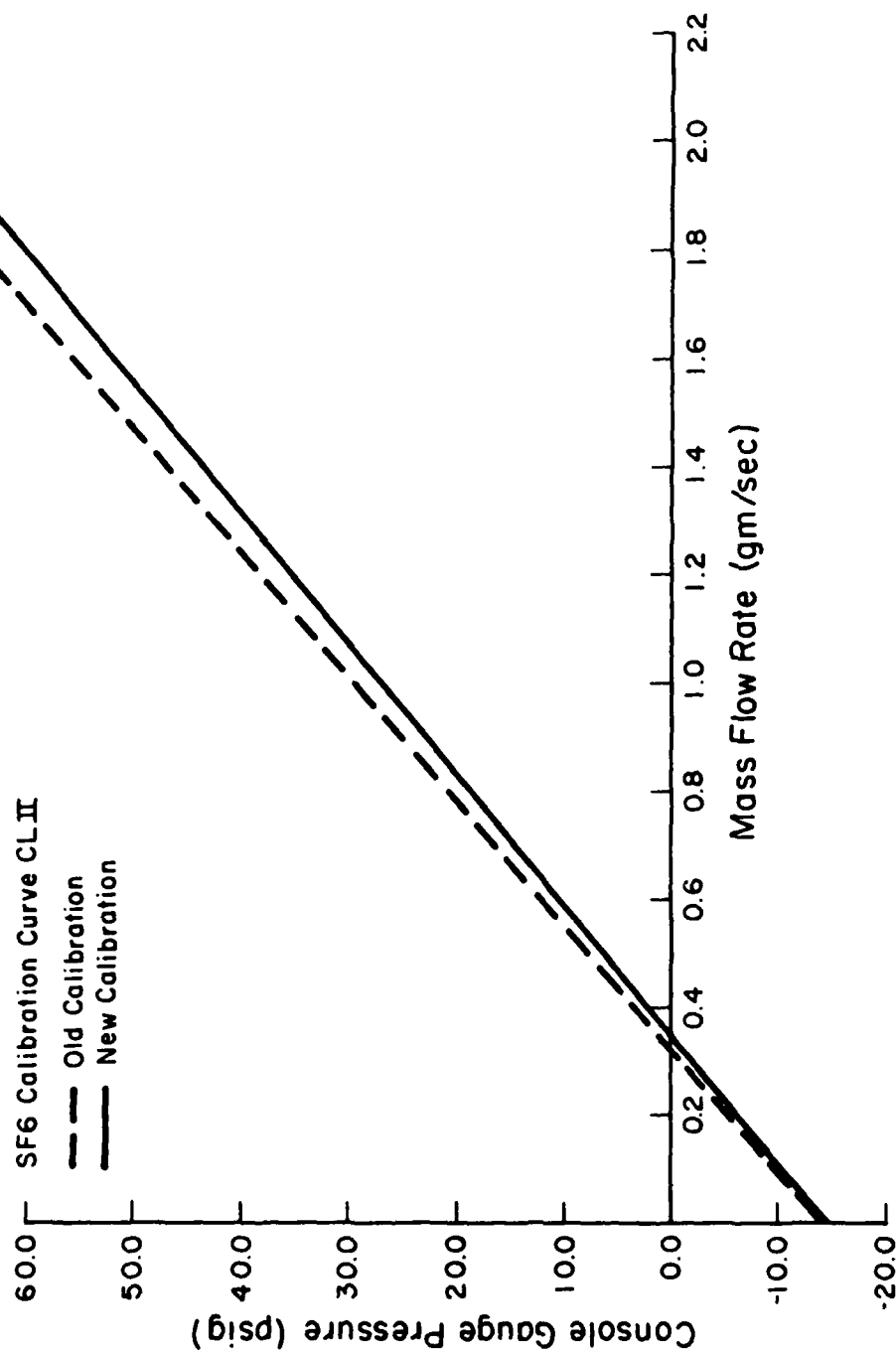
Console Gauge Pressure (psig)

Figure 30. Comparison of the present and the original SF$_6$ mass flow calibration curves for the CL II.
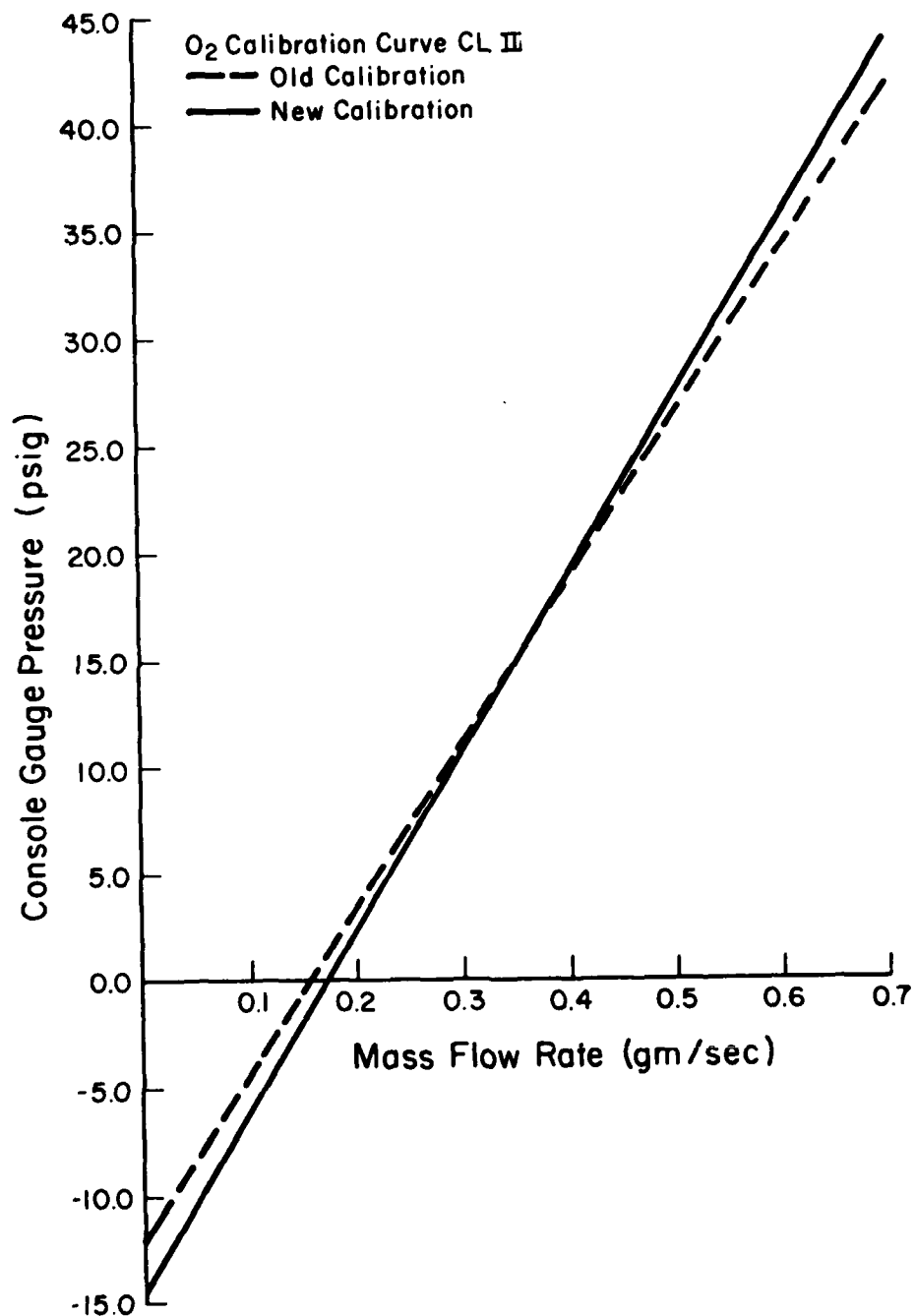
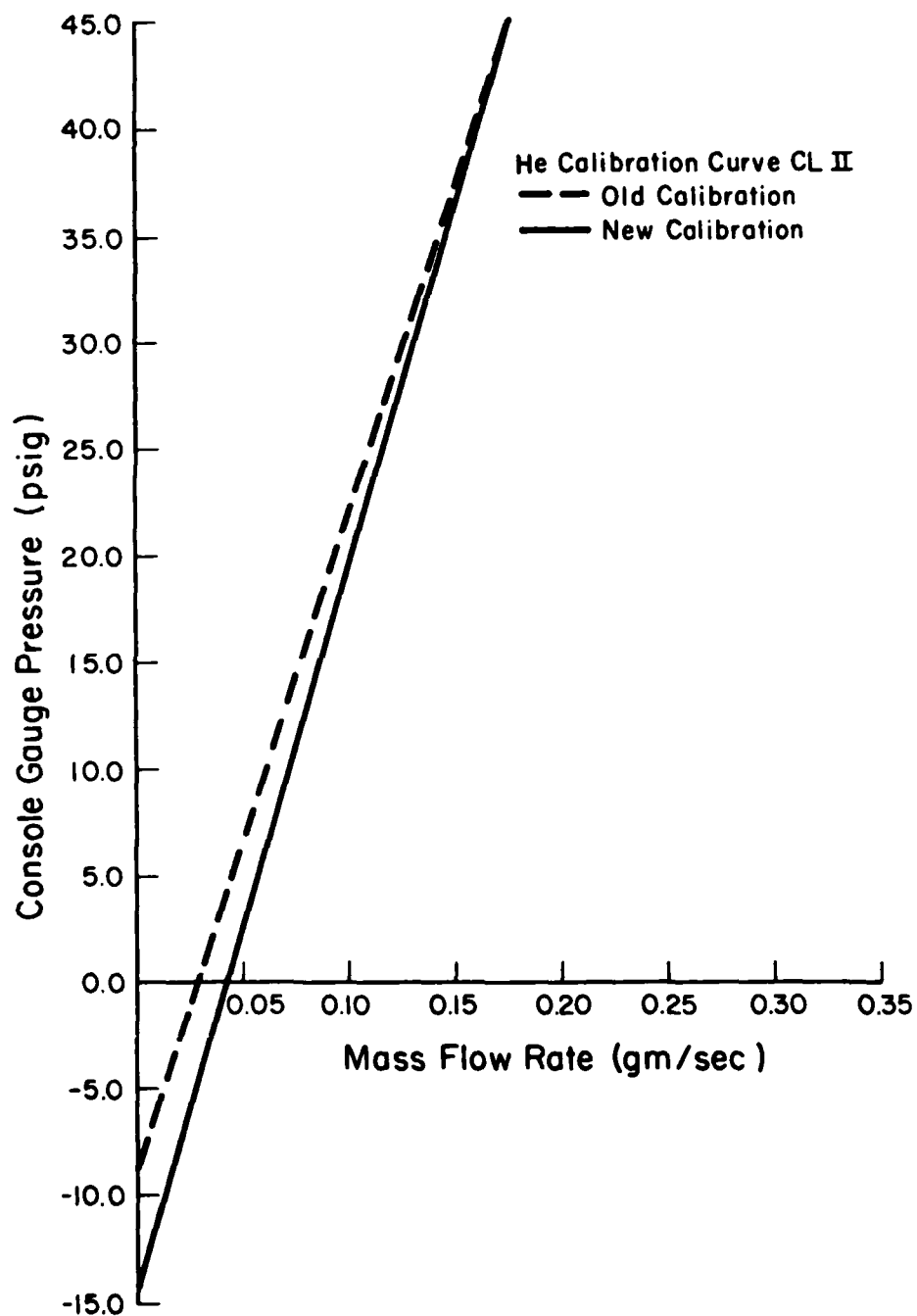Figure 31. Comparison of the present and the original O_2 mass flow calibration curves for the CL II.

Figure 32. Comparison of the present and the original He mass flow calibration curves for the CL II.

IV. CONCLUDING REMARKS

The Micro Motion mass flow meter is a unique device that gives a direct measurement of the mass flow of the fluid passing through it. To the best of our knowledge, it is the only mass flow meter that measures mass flow directly. With this instrument, console pressure versus mass flow rate calibration curves were determined for the four input species H_2, SF_6, O_2 and He for the Helios CL I and CL II laser control consoles. With these curves, the mass flow corresponding to a given console pressure or the console pressure required to obtain a given mass flow rate can be determined.

In the process of generating the calibration curves, several interesting phenomena were observed. To prevent choking of the mass flow meter and control of the mass flow rate by the mass flow meter, the mass flow meter must be inserted into the flow system upstream of the flow control orifice. For some species, in our case H_2, very thin flow control orifices were required to avoid a transition from laminar to turbulent flow in the orifice in the range of mass flow rates of interest. Since the slope of the console pressure versus mass flow rate curve is independent of the zero setting of the mass flow meter, calibration curves can be corrected for errors in the zero setting by sliding the calibration curves horizontally until the extrapolation to zero psia console pressure passes through zero mass flow rate.

REFERENCES

1. MicroMotion Model C Mass Flow Meter Interaction Manual, MicroMotion, 7070 Winchester Circle, Boulder, CO 80301.

2. Shapiro, H. "The Dynamics and Thermodynamics of Compressible Fluid Flow, Vol. I," J. Willey & Sons, N.Y., 1953, pg. 84.

3. Schlichting, H., "Boundary-Layer Theory," 7th ed., McGraw-Hill, N.Y., 1979, pg. 86.

4. Schlichting, H., "Boundary-Layer Theory," 7th ed., McGraw-Hill, N.Y., 1979, pg. 617, deduced from Fig. 20.18.

5. Schlichting, H., "Boundary-Layer Theory," 7th ed., McGraw-Hill, N.Y., 1979, pg. 597.

6. Schlichting, H., "Boundary Layer Theory," 7th ed., McGraw-Hill, N.Y., 1979, pg. 242.

7. Schlichting, H., "Boundary-Layer Theory," 7th ed., McGraw-Hill, N.Y., 1979, pg. 140 and 638.

8. Sentman, L.H., Mosebach, W.O. and Renzoni, P., "A Theoretical and Experimental Study of CW HF Chemical Laser Performance," TR AAE 81-8, UILU Eng 81-0508, Aeronautical and Astronautical Engineering Department, University of Illinois, Urbana, Ill., December, 1981.

END

12-86

DTIC